The Application of Computational Fluid Dynamics to Predict Clinical Outcome of Renal Angioplasty in Patients with a Stenosed Renal Artery

Master thesis Technical Medicine

Ellen van Hulst

UNIVERSITY
OF TWENTE.

The Application of Computational Fluid Dynamics to Predict Clinical Outcome of Renal Angioplasty in Patients with a Stenosed Renal Artery

Graduation comittee

Chair:	Dr. ir. R. Hagmeijer
Medical supervisor:	Prof.dr. B.J.H. van den Born
Technical supervisor:	Dr. K. Jain
Daily supervisor:	L. van de Velde MSc.
Process supervisor:	Drs. R.M. Krol

Defense: 28th November 2022 - University of Twente

"Simulation failed"
by Simvascular

Abstract

Objectives: Identification of patients with renal artery stenosis (RAS) that will respond to renal angioplasty treatment is an ongoing challenge. Patient specific information on the renal haemodynamics could provide insights that may contribute to clinical decision making. Computational fluid dynamics (CFD) is a promising method to determine patient-specific pressure and flow profiles. In this thesis the use of CFD technology in the determination of patient-specific intrarenal pressure and flow parameters will be assessed under resting and hyperaemic conditions to predict blood pressure and kidney function outcomes after renal angioplasty.

Method: A statistical analysis was performed to estimate hyperaemic renal artery flow and renal flow reserve (RFR). A developed CFD model with population averaged and geometric based boundary conditions was validated in 6 patients with RAS. Different simulation methods were explored. Simulated renal fractional flow reserve (rFFR) and translesional pressure gradients were compared to their invasively measured counterpart. In an external data set of 11 patients, simulation results were compared to clinical outcome of renal angioplasty.

Results: Hyperaemic renal artery flow and RFR could not be estimated using patient characteristics and the already existing and frequently used parameters to quantify kidney function. The CFD analysis showed that the mean difference between the most accurate simulation method and measurements was -0.013 $\pm$ 0.028 for rFFR value and 1.11 $\pm$ 2.26 for translesional pressure gradient. The application of the CFD model in the external data set showed a larger clinical response to renal angioplasty in the 5 patients with a rFFR > 0.9 compared to the 6 patients with a rFFR ≥ 0.9.

Conclusions: The application of CFD in the renal arteries has the potential to be of great benefit in the selection of patients for renal angioplasty treatment

in the future. The results provided in the current thesis demonstrate that CFD is suitable for the non-invasive assessment of renal haemodynamics. Future research should show whether the haemodynamic parameters are appropriate to improve patient selection, in which improved CFD models can accelerate the process.

Contents

List of Figures

List of Tables

Glossary

ACE	Angiotensin converting enzyme
ASTRAL	Angioplasty and stenting for renal artery lesion
BMI	Body mass index
BSA	Body surface area
CEUS	Contrast-enhanced ultrasound
CFD	Computational fluid dynamics
CORAL	Cardiovascular outcomes with renal atherosclerotic lesions
CTA	Computed tomography angiography
ERPF	Effective renal plasma flow
FMD	Fibromuscular disease
GFR	Glomerular filtration rate
HERA	Functional renal hemodynamics in patients with renal artery stenosis
MAP	Mean aortic pressure
Pa	Aortic pressure
Pd	Distal pressure
PTA	Percutaneous transluminal angioplasty
PTRA	Percutaneous transluminal renal angioplasty
RAS	Renal artery stenosis
RBF	Renal blood flow
rFFR	Renal fractional flow reserve
RFR	Renal flow reserve
RPF	Renal plasma flow
SNGFR	Single nephron glomerular filtration rate
STAR	Stent placement and blood pressure and lipid-lowering for the prevention of progression of renal dysfunction caused by atherosclerotic ostial stenosis of the renal artery
VCF max	Maximum voluntary contraction force

0

Introduction

Renovascular disease accounts for 1 to 5 percent of all cases of hypertension in the general population and is one of the most common causes of secondary hypertension (5). In 90 percent of the cases, renal artery stenosis (RAS) is caused by atherosclerotic processes (6). Fibromuscular dysplasia (FMD) accounts for the majority of the remaining 10 percent (4, 7). Blood flow through the renal artery can be recovered by a minimally invasive endovascular procedure called percutaneous transluminal renal angioplasty (PTRA). Recent randomised control trials have failed to demonstrate the clinical success of PTRA in addition to medical therapy compared to medical therapy alone regarding improvement of blood pressure control, renal or cardiovascular outcomes. Due criticism can be made of these randomised controlled trials with a major problem being the underrepresentation of the population with "high-risk" clinical presentations, who are more likely to benefit from PTRA (8, 9). Recent observational studies however indicate that there is a subgroup of patients who significantly profit from restoring renal circulation. To date, it has not been established how to identify patients who benefit from revascularisation. Information on the renal haemodynamics could provide relevant insights in the significance of the stenosis.

The currently used diagnostic methods provide limited information on pressure and flow parameters in the renal artery. A promising method to determine patient-specific pressure and flow profiles is computational fluid dynamics (CFD) simulations. Information on the translesional pressure gradient between the pressure distal from the stenosis and the aortic pressure, the renal fractional flow reserven (rFFR), defined as the ratio between distal pressure and aortic pressure can be derived from these simulations. Assessment of these pressure values has shown to significantly improve clinical outcomes in the coronary arteries. Recent developments in CFD technology show the great potential of this technique in the non-invasive assessment of stenosis. Taylor et al. (10) elaborate on the application of

the CFD technique in the simulation of the coronary FFR non-invasively using computed tomography angiography (CTA) data. CFD simulations can provide information on these functional parameters in a non-invasive measure. However, CFD models require patient-specific data as input, which is often unavailable or inadequate. Besides the complexity of the computational model needs to be confined in order to make the simulations clinically feasible. Therefore, assumptions and simplifications are inevitable, which could influence the accuracy of the CFD model.

In the HERA3 study patients scheduled for PTRA undergo invasive intrarenal measurements of the pressure and flow velocity in resting and hyperaemic states during intervention. Hyperaemia can be induced by an intrarenal bolus of dopamine. In addition to the aforementioned pressure parameters, the renal flow reserve (RFR), defined as the ratio between hyperaemic and resting flow velocity, is being determined. The RFR provides information on the microvasculature of the kidney. A study by van de Hoef et al. (11) has shown that in the coronary arteries the combination of coronary FFR and coronary flow reserve has the highest predictive value compared to the predictive value of these parameters separately. The predictive value of these pressure and flow velocity parameters in the renal arteries on hypertension is currently unknown. The invasive intrarenal pressure measurement can be used to validate the accuracy of CFD simulations. Then the developed CFD model can be applied to other data sets to determine the predictive value of pressure parameters. Since the RFR can provide information on the status of the kidneys microvasculature which is believed to play a role in the pathogenesis of renovascular hypertension, and the hyperaemic flow can be used to set up the CFD model, finding a non-invasive measure for the RFR and hyperaemic flow velocity is also attempted. Therefore, the aim of this thesis is to assess the use of CFD technology in the determination of patient-specific intrarenal pressure and flow parameters under resting and hyperaemic conditions to predict blood pressure and kidney function outcomes after PTRA. An overview of the study objectives of this thesis can be seen in figure 1.

The thesis has been divided into five chapters. The first chapter presents the relevant background on RAS and CFD. Chapter 2 addresses a statistical analysis to estimated baseline flow velocity, hyperaemic flow velocity and RFR. Chapter 3 examines the best settings for renal artery CFD simulations and the influence of several input parameters on the outcome. The fourth chapter is concerned with the comparison between simulated and measured values aqcuired during the HERA3 study. In the last chapter, the predictive value of simulated pressure values is examined in an external data set.

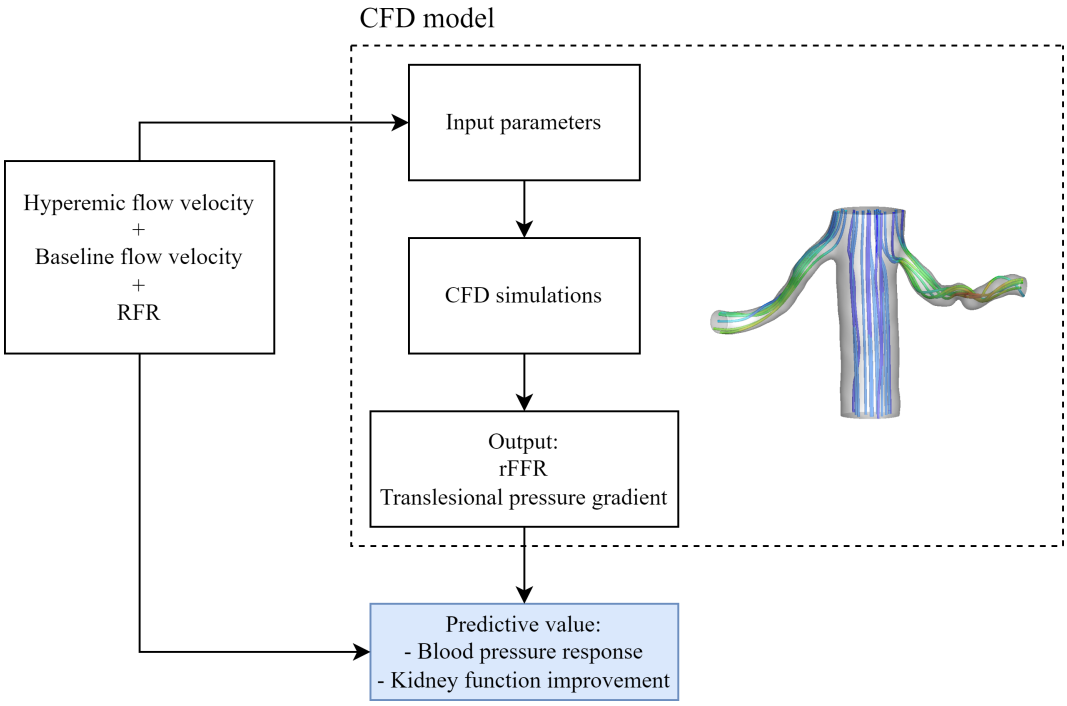

Figure 1: Flowchart of study objectives

1

Background

1.1 Physiology of the Kidney

The human kidney contains about one million nephrons, which are the functional units of the kidney (12). A nephron consists of a glomerulus, a cluster of blood vessels, and a tubule. A schematic representation of a nephron can be seen in figure 1.1. The most important function of the kidneys is filtering blood, which takes place in the renal corpuscle. Blood enters the glomerular capillaries in the renal corpuscle via an afferent arteriole. Glomerular hydrostatic pressure forces about 20 percent of the blood volume into Bowman's capsule and the residual 80 percent is transported further along by the efferent arteriole (12). The filtrate passes through the nephron where reabsorption of substances back into the blood and secretion of extra waste products in the tubule take place. Over 99 percent of the filtered volume is reabsorbed in the proximal tubule (12). Waste products are subsequently excreted in the form of urine to filter the blood and maintain a homeostatic environment.

The filtrating functions can be affected by kidney disease. Multiple conditions affect the kidneys and their functions in different ways. Clinicians use two measures to evaluate the filtering function of the kidneys, the Glomerular Filtration Rate (GFR) and the Effective Renal Plasma Flow (ERPF). The GFR is the volume that is filtered in the glomerular capillaries per unit of time. So this measure assesses the ability of the kidney to filtrate and can be estimated by measuring the concentration of creatinine in serum or as the ratio between the concentration in serum and urine. The GFR is the total glomerular filtration rate, whereas the glomerular filtration rate for a single nephron is the SNGFR. A single nephron filtrates approximately 80 nl/min, which is a fraction of the GFR of 100 ml/min on average (13, 14). The ERPF is the total amount of plasma (1-hematocrit) that passes through the kidneys per unit of time.

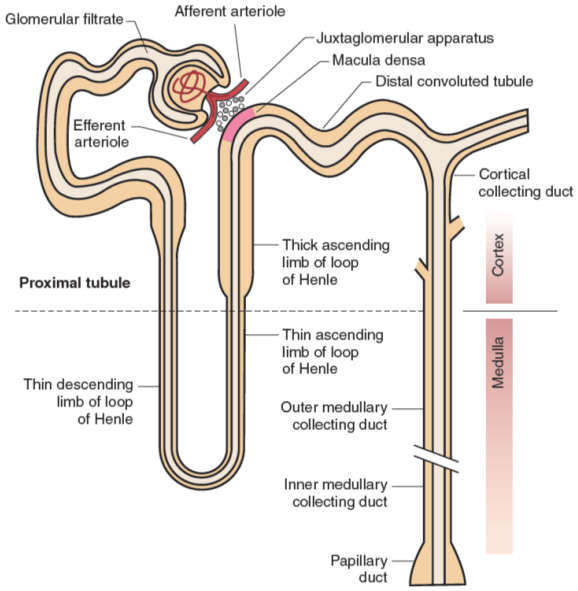

Figure 1.1: Anatomy of the nephron (1).

Another main function of the kidneys is to regulate systemic and renal haemodynamics by the production, secretion, and activation of hormones. Long-term blood pressure regulation is carried out by the renin-angiotensin-aldosterone system (RAAS). When renal blood flow is reduced, the juxtaglomerular cells in the kidney will respond to the decrease in pressure by the excretion of renin in the circulation. Renin, on its turn, converts the pre-enzyme angiotensinogen produced by the liver into angiotensin I. Subsequently angiotensin I is converted to angiotensin II by the angiotensin-converting-enzyme (ACE) present in the pulmonary capillary bed. Angiotensin II has a stimulating effect on sympathetic activity and vasoconstriction. In addition, angiotensin II promotes the secretion of ADH by the pituitary gland and of aldosterone by the adrenal gland. Both ADH and aldosterone act on the kidneys and cause them to retain water. The combined effect of these mechanisms causes blood pressure to increase. The kidney can compensate for an increase in arterial blood pressure by the mechanism of pressure natriuresis. The kidney increases the excretion of sodium and water to lose fluid and restore normal blood pressure. (1, 12, 15)

1.2 Renal artery stenosis

Blood supply of the kidneys is provided by the renal arteries which branch off of the abdominal aorta. Approximately 20 percent of cardiac output is received by the kidneys. The renal arteries then split into several segmental arteries before entering the kidney. Each segmental artery provides a section of the kidney with blood. Those branches then undergo further divisions until the afferent arterioles are formed. The afferent arteriole enters the glomerulus and forms a network of capillaries where filtration takes place. (16) When one or both of the renal arteries are narrowed this is called renal artery stenosis (RAS), see figure 1.2. Blood flow to the kidney can be restricted due to RAS and in 90 percent of the cases, this is caused by atherosclerosis (6). The remaining ten percent is most often caused by fibromuscular dysplasia (FMD) (4, 7). In an autopsy study by Sawicki (17) in 1991 the prevalence of RAS was found in 4.3 percent of the 5194 performed autopsies, of which 73 percent of those patients were found to be hypertensive. In patients with RAS, perfusion to the kidneys is limited, leading to renal ischemia. The ischemic kidney secretes renin, which leads to an increase in blood pressure. This has been elegantly demonstrated in the Goldblatt experiments (18), where one or two of the renal arteries in dogs were clamped. The contralateral intact kidney, if present, responds to this increase in blood pressure by the excretion of sodium. Hypervolemia is hereby prevented and thus renin levels will stay increased. This leads to a chronic phase of hypertension which is renin-dependent. If however the contralateral kidney is not intact, or the renal arteries on both sides are narrowed, pressure natriuresis can not occur and sodium will be retained. Sodium retention will naturally lead to water retention and plasma volumes will increase. This form of chronic hypertension is called renin-independent hypertension. (19) RAS has often been associated with hypertension and renal deterioration. (4, 20, 21, 22). According to the Dutch RENINE registry (23), in 2019 renal vascular disease has been the primary cause of renal replacement therapy in 6 percent of the patients in the Netherlands.

1.3 Percutaneous transluminal renal angioplasty

To recover blood flow through the renal artery in the case of RAS, percutaneous transluminal renal angioplasty (PTRA) with or without stent placement can be performed. PTRA is often successful and without complications. However, the clinical benefit of PTRA on blood pressure and renal function has been questioned. Several smaller clinical studies performed in the nineties have shown a significant improvement in blood pressure and renal function (22, 24, 25, 26). Subsequently, randomised control trials using a large number of patients have been performed. Of those, the most important are the CORAL (27), ASTRAL (20) and STAR (28) trials. These trials showed that PTRA with stent placement in addition to

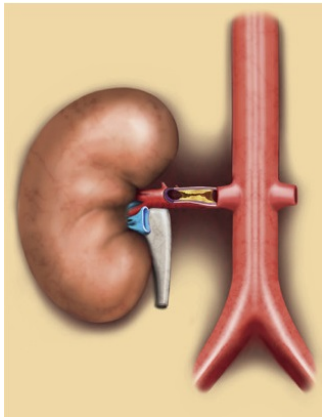

Figure 1.2: Kidney with an atherosclerotic renal artery stenosis (2)

.

medical therapy was not superior to medical therapy alone (29). As a result, renal revascularisation therapy has declined sharply (4).

However, this decline may be out of place, since the inclusion criteria of these studies can be criticised (4, 30). Firstly, patients suffering from uncontrolled or treatment-resistant hypertension were excluded from the studies, despite the expectation that these patients benefit from revascularisation most. Secondly, patients were only eligible if the attending physician doubted the benefit of PTRA. Lastly, due to the slow inclusion of the CORAL trial, the inclusion criteria have been broadened leading to the inclusion of patients with no serious stenosis. It can also be mentioned that the control group was treated with very strict medical therapy, which may not be feasible in clinical practice. Altogether, these factors might have led to the failure of showing a clinical benefit from PTRA. It is still unclear how to identify patients who would benefit from revascularisation (31).

Conventional non-invasive imaging techniques have not been able to identify which individuals may benefit clinically from revascularisation. Experiences in the Amsterdam Medical Centre and recent unrandomised studies however show that there are patients who significantly profit from the treatment (4). Information on renal haemodynamics may help in better understanding the significance of the stenosis. In the coronary arteries, functional characteristics of blood flown have shown to significantly improve the selection of patients who will respond to treatment of coronary artery disease (11). For the renal arteries functional haemodynamic parameters have been evaluated in a limited number of patients (32, 33, 34, 35), leading to promising results.

1.4 Computational Fluid Dynamics

A new clinical application in the analysis of fluid flow problems is computational fluid dynamics (CFD), in which the Navier-Stokes equations are solved in a numerical manner. CFD simulations can provide insight in functional haemodynamic renal pressure parameters in patients with RAS non-invasively. The process of CFD modelling comprises several steps. In the first phase the patient-specific geometry, mesh, boundary conditions, and material properties are set. In the next phase, the settings to perform finite element CFD simulations are determined and the underlying governing fluid equations are solved numerically by the computer. After the simulation, the results can be analysed. The following sections will elaborate on the steps involved in performing a CFD simulation.

Geometry

As the first step, the 3D volume of the vessel lumen needs to be determined. The extensively researched field of image segmentation provides many different techniques to tackle this problem using an automated approach. Often magnetic resonance angiography or computed tomography angiography (CTA) images are used as input to determine the borders of the arterial lumen. Several commonly used segmentation methods are described in the following sections.

2D segmentation method

The 2D segmentation process is build-in in the SimVascular pipeline. First, a path needs to be specified along the arteries of interest. Along the created path, 2D segmentations of the artery need to be created using the interpolated image slices that are perpendicular to the pathline. Both the intensity of the reslice and the magnitude of the intensity gradient are shown. The 2D segmentations can be created automatically using threshold values, or manually by adding points based on visual inspection. The 2D segmented slices can automatically be lofted to create a solid model. For each artery, a separate solid model should be created which then can be merged to create the final model. Lastly, smoothing of the model, especially around the junction of the joined arteries, is needed. The created smoothed model can then be trimmed to the area of interest, creating different faces including the wall and the ends of the arteries. The faces need to be appointed as a wall or cap, whereafter appropriate remeshing can be applied.

3D Level set method

A more sophisticated method less prone to user dependency is the built-in 3D level set method (36). The surface of the 3D model corresponds to the largest intensity magnitude gradient. The first initialization of the surfaces can be obtained using the colliding fronts

method (37). For this, seed points are placed at the start and end of the artery. Two wavefronts propagate from the seeds, with the speed proportional to the image gradient. The region where the wavefronts coincide in propagation direction is defined as the initial level set deformable surface. The numerical equations of the mathematical framework are then solved multiple times to achieve the final deformable surface. Different weights can be specified to adjust surface evolution.

3D segmentation based on threshold
A segmentation can be created in an automated manner by using the threshold values of the image intensity. In the region-growing method, the users place a seed in the arteries of interest. The region grows from the selected seed including all the regions within the values of some specified thresholds. Another method to indicate the area of interest is by creating a mask before threshold segmentation. Within the mask threshold segmentation can be applied. Mistakes in the segmentation can be adapted manually or by using more automated tools. The segmentation can be turned into a polygon model, and appropriate smoothing and trimming steps need to be applied.

Meshing

The created solid 3D model needs to be divided into small subdomains, a process called discretization or mesh generation. An example of a mesh created for a renal artery stenosis can be seen in figure 1.3. Later in the simulating phase, the numerical equations will be solved for all nodes in the mesh for a given number of time steps. A commonly used shape element for 3D volumes is the tetrahedral element. Tetrahedral elements are organised in an unstructured manner and are therefore able to capture complicated domains, such as arteries. In the mesh generation process, it is intended to find the coarsest mesh, still fine enough to produce reliable simulation results. A specific addition for arterial meshing is the addition of a boundary layer at the walls of the domain. In fluid dynamics, the no-slip condition for viscous fluids presupposes that the fluid will have zero velocity relative to the wall (38). The velocity and pressure gradients near the wall are therefore large, which can be more accurately simulated by the increased density meshing of the boundary layer.

In order to reduce computational time, radius based meshing can be applied. In this method the global edge size of the mesh is adapted scaled to the radius of the artery. This is esspecially beneficial in stenotic arteries, since the fine meshing needed in this area is not applied in the coarser areas such as the aorta. The radius based meshing method will compute the centerlines and find the distance to the centerlines prior to meshing. The global max edge size is multiplied by the normalized values of these distances.

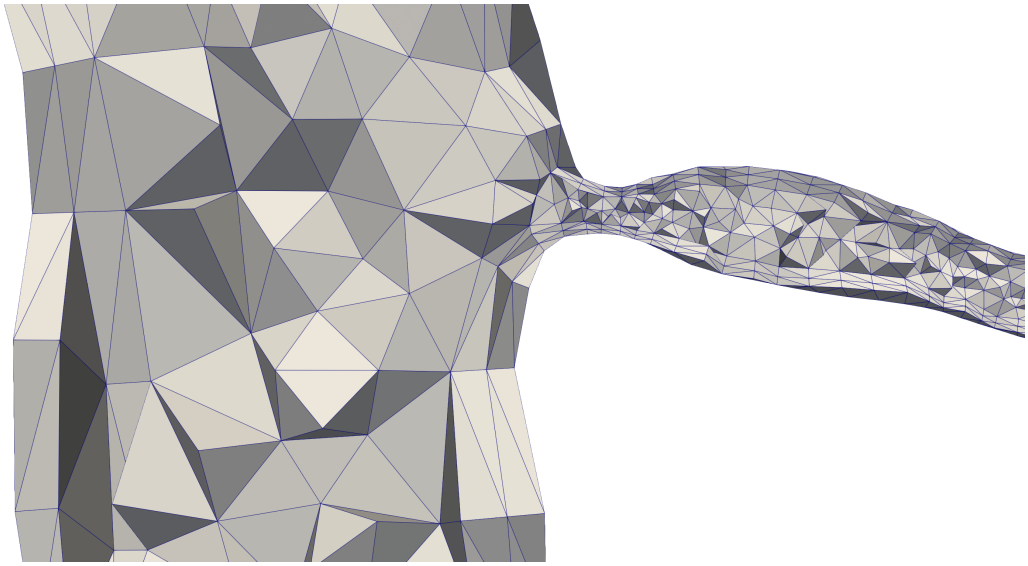

Figure 1.3: Example of a tetrahedral mesh of a renal artery stenosis. The mesh was created in SimVascular using boundary layer meshing and radius based meshing.

Boundary conditions

The boundary conditions connect the model with its surroundings. In the case of arterial simulations, the boundary conditions need to capture the physiology of the vascular network. Wall motion can included or neglected, which is called a rigid wall. In this thesis, only rigid wall simulations are performed.

Inlet

The inlet is defined as the face where the fluid enters the geometric model. It can be specified by giving a flow rate or a pressure value. Both static inflow conditions and pulsatile conditions are possible. Estimations for the inflow conditions can be made based on known information about physiology, or patient-specific measurements.

Outlet

The outlet boundary conditions represent the more distally located vasculature outside the domain including smaller arteries, arterioles, capillaries, venules, and veins. A relation between pressure and flow can be prescribed by a resistance. The resistance will primarily be determined by the resistance of the arterioles since the largest pressure drop happens there (15). The relation is applied weakly, meaning that the integral of the outlet velocities must satisfy the relation.

Material properties

The material properties of the fluid simulated need to be defined. The properties of blood can be described by its viscosity and density.

Viscosity

Viscosity (μ) is an intrinsic property of fluid and is a measure of the fluids resistance to flow. Blood is a non-Newtonian fluid, meaning that the viscosity is dependent on shear rate. The non-Newtonian properties of blood are caused by the interaction between fibrinogen and red blood cells, and is dependent on factors like temperature, fibrinogen concentration, hematocrit values, the radius of the vessel, and linear speed. At high shear rates, however, the behaviour of blood is like a Newtonian fluid, and can therefore be simulated like one. (15) In arteries the viscosity can be represented by a constant. The normal range for blood viscosity is between 3.5 and 5.5 centipoise (39).

Density

Blood density (ρ) depends on the total protein concentration and is proportional to its hematocrit value (40). The density of blood is close to the density of water. Literature suggests values between 1043 and 1060 kg per m^3 (41).

CFD Solver

After defining all the conditions for the simulation, the simulation tool can perform the simulation by solving the three-dimensional incompressible Navier-Stokes equations, the governing equations of blood flow. The Navier-Stokes equations are two partial differential equations that describe the flow of incompressible fluids. The equations express the conservation of mass and Newton's second law, the conservation of momentum, and are in the form:

$$\nabla \cdot u = 0$$

$$\rho \left(\frac{\partial u}{\partial t} + (u \cdot \nabla)u \right) = -\nabla p + \mu \nabla^2 u + F$$

Where u is the velocity vector, t is time, ρ the density of the fluid, p the pressure, μ the viscosity of the fluid and F the external forces. Simulations can be performed with the SimVascular finite element solver (42).

1.5 HERA studies

In 2014 the first Functional Renal Haemodynamics in Patients with Renal Artery Stenosis (HERA) study was started, followed by HERA 2 and HERA 3, which started in 2019 (3). The HERA studies aim to find the clinical value of invasive pressure and flow measurements in the renal artery to predict the expected benefit for patients undergoing renal revascularisation. In patients scheduled for percutaneous transluminal angioplasty (PTA), invasive intrarenal measurements of the pressure and flow velocity will be performed during the intervention. For measurements, a 0.014" dual doppler and pressure sensor-equipped guide wire is being used. In all three studies, renal artery blood flow velocity is measured during baseline and during hyperaemia. In the first HERA study the reproducability of the flow and pressure measurements in the renal artery using a flow wire was examined. Patients with an indication for PTA, in the coronary or other arteries, were included in this study. The subjects for this study did not necessarily have RAS. A total of 41 subjects were included. The second HERA study aimed to assess the effect of the handgrip maneuver on the renal artery flow. During this maneuver the sympathic nerves system is stimulated leading to a decrease in renal artery flow. In the HERA 2 study 29 patients were included. Lastly the HERA 3 study included only patients going for PTA in the renal artery. The aim of this study is to find the predictive value of the pressure and flow measurements in the renal artery. At the timing of conducting this study, 14 patients were included in the HERA 3 study of which eight had successful renal artery measurements. In addition to the invasive measurement, 24-h ambulatory blood pressure measurements and ERPF/GFR measurements are performed before and three months after the intervention to assess the gained improvement in blood pressure and renal function. Also, urine and blood samples are taken. For an overview of the study procedures, see figure 1.4. The aim is to have included 30 patients by the end of 2022. Currently, 19 patients have been included and have undergone pressure-flow measurements. Based on the pressure-flow measurements several haemodynamic parameters can be determined. The utility of these parameters in the coronary arteries has already been demonstrated (11), which gives high hopes for their predictive value in the renal arteries (4).

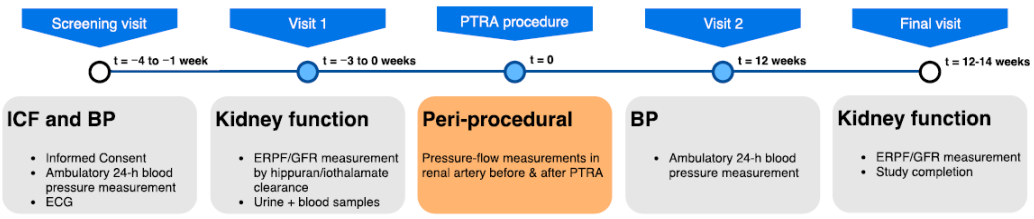

Figure 1.4: Flowchart of the HERA 3 study procedure (3)

Translesional pressure gradient

Previous research has shown that anatomical grading of stenosis is not sufficient in describing its severity (4, 11). The significance of stenosis, therefore, needs to be determined using a different parameter. The translesional pressure gradient is defined as the mean proximal pressure minus the mean distal pressure over the stenosis. The proximal pressure is equal to the aortic pressure and therefore:

$$Translesional\ pressure\ gradient = P_{aortic} - P_{distal}$$

It, therefore, describes the pressure drop caused by the stenosis. The translesional pressure gradient will be determined in both resting and hyperaemic conditions.

Renal fractional flow reserve

The renal fractional flow reserve (rFFR) quantifies the haemodynamic significance of the stenosis by its limiting effect on maximal flow. In a study by Pijls et al. (43) it was shown with a simplified model that the FFR in the coronaries can be determined from pressure measurements during hyperaemic conditions. Therefore the rFFR can be determined as the ratio of distal to proximal pressure during hyperaemic conditions.

$$rFFR = \frac{P_{distal}}{P_{aortic}}$$

Renal flow reserve

The lack of success in PTRA found in the randomised control trials may be due to dysfunctional microvasculature in the kidney (44). A parameter that can indicate the condition of the renal microvasculature is therefore needed. The renal flow reserve (RFR) is the increase in intrarenal flow velocity after maximal vasodilatation. It thereby reflects the microvascular function of the kidney. Using the ComboWire (Philips-Volcano, San Diego, US) the flow velocity in the renal artery will be measured in resting and hyperaemic conditions. By the infusion of dopamine in the renal artery, maximal vasodilatation (hyperaemia) is induced (29). The RFR is then defined as the ratio of the temporally averaged peak flow velocity in hyperaemic conditions to the temporally averaged peak flow velocity in rest.

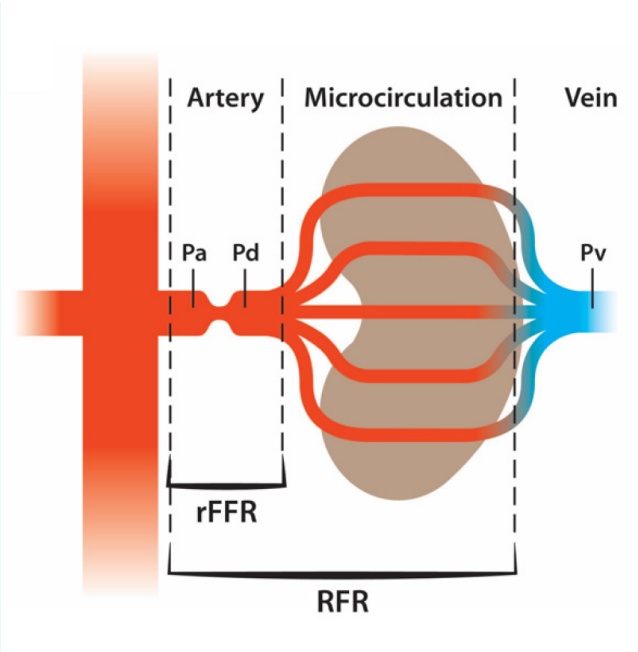

Figure 1.5: The functional parameters on RAS. Pa = aortic pressure; Pd = distal pressure in the renal artery; Pv = pressure in the renal vein; rFFR = renal fractional flow reserve; RFR = renal flow reserve (4)

2

Renal Flow Reserve

2.1 Introduction

RAS is often associated with deteriorated microvasculature of the kidney. Interstitial fibrosis develops as a result of a prolonged decline in renal perfusion (30, 45). Additionally, in ARAS, the atherosclerotic processes causing the stenosis might also affect the intrarenal vessels directly (46). High cholesterol feeding plays an important role in the acceleration of microvascular decline in ARAS (45, 47). Several other processes, such as inflammatory pathways, contribute to the reduced vasculature distal from the stenosis as shown by experimental studies (45). These structural alterations in the microvasculature may be a possible explanation for poor response to treatment (48). Assessment of the renal mircorvasculature might therefore lead to improved patient selection for PTRA. The RFR, defined as the ratio between hyperaemic average peak velocity and baseline average peak velocity, is a measure for the state of the microvasculature. The hyperaemic average peak velocity can be obtained by injecting a bolus of dopamine in the renal artery during angioplasty. The hypothesis is that the RFR, combined with the rFFR, is a good predictor for the response in blood pressure and kidney function after PTRA.

To date no non-invasive measure of the RFR is available. It would be desirable to assess hyperaemic renal artery average peak velocity and the RFR non-invasively for multiple reasons. Firstly because the RFR provides information on microvasculature kidney status, and could therefore contribute to the decision-making for treatment prior to angiography. Secondly, the CFD model developed in the current thesis, which will be explained in a later chapter, uses hyperaemic flow rate to set an outlet boundary condition. A non-invasive estimation of hyperaemic flow rate could therefore improve accuracy of the simulations. Therefore, the current study aims to find a clinical predictor for the RFR, hyperaemic and baseline renal average peak velocity.

2.2 Method

Data collection

The data collected during the HERA 1, HERA 2 and HERA 3 study were used. A total of 84 patients were included. Data included demographic characteristics, medical history, physical characteristic and urinary and blood sample values. In all three studies, renal artery blood average peak velocity is measured during baseline and during hyperaemia. Some additional clinical data were retrieved from the electronic health record. The Body Surface Area (BSA) was calculated using the Du Bois formula. Kidney length was measured on ultrasound images, or on CTA scans.

Invasive Measurements

Since the start of the HERA 3 study 19 patients scheduled for renal revascularisation were included in the study. During the procedure various intrarenal pressure and flow measurements were performed. Access was obtained via the groin into the femoral artery. Using a guide wire, the stenosis is passed and the flow wire is then placed distal from the stenosis, where the blood average peak velocity and pressure is measured. The pressure was also measured at the location of the tip of the catheter, which is placed proximal from the stenosis. When the catheter and wire are in a fixed position and a stable signal can be acquired, multiple measurements will be performed. The first measurement is during baseline flow, and will be recorded for 5 minutes. During the next measurement, the dynamic handgrip test is performed for 3 minutes, followed by 5 minutes of the static handgrip test. The dynamic handgrip test involves the subject to alternate between contraction of the handgrip and relaxation every 6 seconds. Contractions will be at 40 percent of individual maximum voluntary contraction force (VCF max). The subjects contract the handgrip to a maximum of 20 percent of individual maximum voluntary contraction force for 5 minutes during the static handgrip test. Lastly a hyperaemic measurements will be performed for 5 minutes. To induce the hyperaemic state, the subject is injected with a dopamine bolus of 30 µg/kg directly in the renal artery. The hyperaemic renal average peak velocity can be used to determine the RFR of the subject. The rFFR is determined using the pressure measurements during the hyperaemic state. In the first two HERA-studies, measurements comparable to the measurements described above were performed.

Signal analysis

Pressure and flow signals were stored and analysed offline using functions created in MATLAB (R2022b, The Mathworks, Inc. Natick) for previous HERA studies. Firstly an interval of approximately 10 beats is selected. One segment during baseline flow, and one segment at hyperaemic velocity after injection of the dopamine bolus of 30 µg/kg. Secondly, a 4th order

Savtizky-Golay filter is applied to the signals and the velocity signals were shifted backwards 50 ms. From the signal averaged pressure and velocity parameters were computed.

3D segmentation kidney

Kidney volume might be a good predictor for status of the microvasculature, since kidney volume decreases in patients with decreased kidney function (49). To gain the volume of the kidney, 3D segmentation of the kidneys anatomy from CTA images was done. In 3D slicer (50), a free and open-source platform for analysing and understanding medical image data, CTA scans were loaded and segmented. Firstly a volume mask was created around the kidney concerned. Within the volume mask the kidney was segmented using a threshold range. Due to differences in imaging settings, the border between renal cortex and renal core was not always clearly visible and seemed to differ fairly between kidneys. Accordingly, it was chosen to fill in the core of the kidney including the renal pelvis. Impurities in the segmentation were removed using a manual eraser tool. Lastly smoothing of the volume was applied using a Gaussian smoothing filter.

Statistical analysis

Statistical analysis was performed using R version 4.0.3 (R Foundation, Vienna, Austria). The shapiro-Wilk's test was used to test the outcome measures RFR, baseline average peak velocity and hyperaemic average peak velocity, and all the clinical parameters for normality. Accordingly, a baseline table of all the parameters is created using the mean and standard deviation for normal distributed parameters and the median with interquartile range for not-normal distributed parameters. Univariate linear regression analysis was performed on the numerical parameters to find the relevant clinical parameters for determining the RFR, baseline average peak velocity and hyperaemic average peak velocity. The parameters leading to a p-value < 0.3 were selected. The categorical data were compared using an unpaired t-test assuming normal distribution based on the central limit theorem. This theorem tells us that the sample distributions is approximately normal for large enough sample sizes ($n>30$), for which the t-test can be applied (51).

After determining the relevant parameters for the prediction of the RFR, baseline average peak velocity and hyperaemic average peak velocity, an attempt was made to develop a multivariate model. A multivariate model was created using the backward elimination method. Firstly all the parameters which had a p-value below 0.3 in the univariate regression analysis were taken. The parameters concerning renogram, kidney length, kidney volume and renal artery diameter were excluded, because it reduces the number of patients left for analysis profoundly. Parameters which were retrieved during the invasive measurements were also excluded. Then the parameter with the highest p-value in the multivariate model was re-

moved and the multivariate regression was performed again. This step was repeated until 3 parameters were left in the model. The error rate is calculated by dividing the residual standard error by the mean outcome variable. The multivariate models created in the previous step was taken and compared to the same model with the addition of one of the parameters concerning renogram, kidney length or renal artery diameter. The resulting models were compared using the analysis of variance (ANOVA) function. A p-value below 0.05 indicates that the more complex model is significantly better than the simple model.

An univariate linear regression analysis was also performed to determine the added value of the parameters regarding kidney volume and renogram in addition to kidney length parameters. The two methods used to measure kidney length, on ultrasound images and on CT images were also compared.

2.3 Results

This section contains the baseline characteristics of the patients. It also shows the results of the statistical analysis performed.

Baseline data
The baseline characteristics of the clinical parameters are shown in table 2.1. Baseline characteristics were shown for patients with and patients without significant stenosis separately. For each parameter, all the subjects for which this parameter is available were included.

Univariate analysis RFR, baseline and hyperaemic average peak velocity
In tables 2.2, 2.3 and 2.4 the results of the univariate regression analysis and the two-tailed t-tests are shown for the parameters given a p-value smaller than 0.3.

Table 2.1: Baseline characteristics

Parameter	Overall (n=84)	No stenosis (n=66)	Stenosis (n=13)
HERA-study			
HERA 1	41 (48.8)	35 (53.0)	5 (38.5)
HERA 2	29 (34.5)	27 (40.9)	1 (7.7)
HERA 3	14 (16.7)	4 (6.1)	7 (53.8)
Age (years)	56.26±15.04	55.27±15.76	65.00 [50.00, 68.00]
Sex, male	50 (59.5)	43 (65.2)	5 (38.5)
Weight (Kg)	83.00 [74.08, 89.75]	84.00 [76.00, 90.00]	75.98±16.40
Length (cm)	174.00 [168.00, 181.00]	174.50 [168.50, 181.00]	171.00 [163.00, 172.00]
BMI (Kg/m^2)	27.32±3.80	27.60 [25.02, 29.40]	26.50±3.87
BSA (m^2)	1.92±0.36	2.00 [1.89, 2.10]	1.86±0.21
VCF max (kN/m^2)	30.00 [24.00, 38.00]	30.00 [24.00, 38.75]	32.00 [18.00, 38.00]
Ethnicity, caucasian	76 (90.5)	60 (90.9)	11 (84.6)
Smoking			
Current	15 (19.0)	13 (20.3)	2 (16.7)
History	31 (39.2)	25 (39.1)	3 (25.0)
Never	33 (41.8)	26 (40.6)	7 (58.3)
History of diabetes mellitus	23 (28.0)	19 (28.8)	4 (30.8)
History of cardiovascular disease	49 (59.8)	39 (59.1)	10 (76.9)
Hemoglobin (mmol/L)	8.30 [7.88, 8.80]	8.30 [7.90, 8.90]	8.15 [7.70, 8.50]
Serum potassium (mmol/L)	3.88±0.31	3.90 [3.70, 4.00]	3.90 [3.40, 4.10]
High Density Lipoprotein (mmol/L)	1.19±0.41	1.16±0.41	1.27 [1.16, 1.35]
Low Density Lipoprotein (mmol/L)	2.37±0.90	2.17 [1.76, 2.69]	3.13 [1.68, 3.69]
Triglycerides (mmol/L)	1.43±0.93	1.45±0.98	1.69 [0.85, 1.80]
HbA1c (mmol/mol)	41.24±9.39	41.16±9.86	41.00 [35.00, 44.00]
Serum aldosterone (nmol/L)	0.13±0.17	0.12±0.16	0.18±0.24
Urine Creatinine (mmol/L)	9.87±6.40	10.49±6.73	7.80 [3.65, 9.90]
eGFR ($mL/min/1.73m^2$)	78.30±19.01	87.00 [70.25, 92.75]	66.00 [50.00, 74.00]
Mean arterial pressure (mmHg)	101.56 [94.35, 111.06]	101.33 [94.35, 108.97]	107.11 [101.00, 115.22]
Renogram ipsilateral* (%)	54.00 [50.00, 56.00]	55.00 [50.00, 56.00]	52.50 [50.25, 56.50]
Kidney length ipsilateral* (cm)	10.50 [9.75, 11.25]	11.00 [10.50, 11.50]	10.25 [9.50, 10.88]
Kidney length contralateral* (cm)	10.50 [10.25, 11.25]	10.50 [10.50, 11.50]	10.75 [9.62, 11.00]
Kidney volume ipsilateral* (cm^3)	149.86 [105.89, 181.83]	167.62 [150.45, 196.04]	110.06 [93.35, 166.44]
Kidney volume contralateral* (cm^3)	154.96 [126.51, 171.66]	169.39 [153.13, 200.57]	144.72 [95.42, 165.21]
Renal artery diameter* (cm)	0.55 [0.48, 0.59]	0.53 [0.47, 0.56]	0.58 [0.49, 0.66]
Baseline flow velocity* (cm/s)	31.83 [27.12, 39.64]	34.71±12.32	25.00 [15.20, 37.96]
Hyperaemic flow velocity* (cm/s)	65.84±24.63	68.56 [52.34, 81.36]	48.56 [39.68, 59.39]
RFR*	2.11±0.74	2.09±0.69	1.84 [1.35, 2.99]

Continues variables are given in mean±SD or median [IQR], catgorical variables are given in number (%).

* Renogram ipsilateral: overall (n=13), no stenosis (n=5), stenosis (n=8); Kidney length: overall (n=27), no stenosis (n=17), stenosis (n=10); Kidney volume: overall (n=8), no stenosis (n=3), stenosis (n=5); Renal artery diameter: overall (n=19), no stenosis (n=10), stenosis (n=9); Baseline flow velocity: overall (n=69), no stenosis (n=59), stenosis (n=10); Hyperaemic flow velocity: overall (n=67), no stenosis (n=57), stenosis (n=10); RFR: overall (n=67), no stenosis (n=57), stenosis (n=10);

Table 2.2: Univariate regression and two-tailed t-tests results for predicting RFR

VarName	Intercept	Coefficient	p-value	r-squared
VCF max	1.82	0.01	0.26	0.02
Serum potassium	0.34	0.45	0.15	0.03
HDL	2.39	-0.24	0.27	0.02
LDL	1.67	0.19	0.06	0.05
Urine creatinine	1.85	0.02	0.13	0.04
Renogram ipsilateral	4.44	-0.04	0.23	0.14
Renogram ratio	3.34	-0.91	0.20	0.16
Kidney length ipsilateral	4.49	-0.22	0.12	0.09
Kidney length absolute difference	2.10	-0.19	0.23	0.06
Kidney length ratio	4.17	-2.06	0.24	0.06
Baseline average peak velocity	2.99	-0.02	<0.01	0.22
Hyperaemic average peak velocity	1.55	0.01	0.02	0.08
VarName	-	-	p-value	t-test statistic value
Ethnicity	-	-	0.2037	1.4057

Table 2.3: Univariate regression and two-tailed t-tests results for predicting baseline average peak velocity

VarName	Intercept	Coefficient	p-value	r-squared
Weight	43.57	-0.12	0.28	0.02
Length	74.34	-0.23	0.18	0.03
BSA	54.10	-10.42	0.19	0.02
Triglycerides	30.18	2.14	0.19	0.03
Aldosterone	34.91	-12.49	0.28	0.02
Renogram ipsilateral kidney	-7.71	0.82	0.26	0.12
Renogram contralateral kidney	73.96	-0.82	0.26	0.12
Renogram absolute difference	33.12	0.41	0.26	0.12
Kidney length ipsilateral	-3.07	3.44	0.20	0.07
Kidney length absolute difference	34.00	4.81	0.10	0.10
Kidney length ratio	-15.00	48.83	0.13	0.09
Hyperaemic average peak velocity	10.84	0.34	<0.01	0.41
RFR	51.36	-8.46	<0.01	0.22
VarName	-	-	p-value	t-test statistic value
Stenosis present	-	-	0.17	1.46
Smoking (ever vs never)	-	-	0.26	1.13

Table 2.4: Univariate regression and two-tailed t-tests results for predicting hyperaemic average peak velocity

VarName	Intercept	Coefficient	p-value	r-squared
Age	83.89	-0.32	0.12	0.04
Length	136.07	-0.40	0.22	0.02
Serum potassium	8.08	14.77	0.16	0.03
Urine creatinine	57.02	0.78	0.12	0.04
Renal artery diameter	104.66	-78.51	0.24	0.08
Baseline average peak velocity	25.51	1.20	<0.01	0.41
RFR	46.08	9.38	0.02	0.08
VarName	-	-	p-value	t-test statistic value
History of CVD	-	-	0.25	1.17
Stenosis present	-	-	<0.01	3.38
Ethnicity	-	-	0.14	1.65

Multivariate analysis

The results of the final multiple regression models including three parameters are shown in table 2.5. The addition of the parameters concerning renogram, kidney length and renal artery diameter did not significantly improve the model based on the ANOVA comparison.

Table 2.5: Multiple regression model exclusive Renogram, kidney length, BL1 and HE1

Outcome Variable	Predictive variables	Adjusted R-squared	p-value	Error rate
RFR	VCF max, LDL, Urine creatinine	0.12	0.04	0.33
Baseline average flow velocity	BSA, Aldosterone, Smoking	0.14	0.01	0.36
Hyperaemic average flow velocity	Age, Length, Ethnicity	0.11	0.02	0.37

Kidney characteristics

Univariate regression analysis was performed between different kidney characteristics. Kidney length measured by ultrasound is strongly correlated to the kidney length measured on CTA. The univariate regression model showed that renal volume is strongly correlated to kidney length. The correlation was highest using the kidney length measured on CTA. The renogram function division can also be predicted using kidney length measured on CTA. For the results see tables 2.6, 2.7 and 2.8.

Table 2.6: Univariate regression results for predicting kidney length measured on CTA using kidney length measured on ultrasound.

Variable	intercept	coefficient	p-value	r-squared
Ultrasound	-0.24	1.05	<0.01	0.78

Table 2.7: Univariate regression results for predicting kidney volume using Kidney lengths.

Variable	intercept	coefficient	p-value	r-squared
Ultrasound	-259.84	39.25	<0.01	0.67
CTA	-213.30	34.01	<0.01	0.80

Table 2.8: Univariate regression results for predicting renogram using kidney lengths.

Variable	intercept	coefficient	p-value	r-squared
Kidney length CTA absolute difference	51.75	7.73	<0.01	0.82
Kidney length CTA ratio	-33.57	85.18	<0.01	0.80

2.4 Discussion

The results show that RFR or hyperaemic average peak velocity are very poorly estimated using solely clinical parameters. The best multivariate regression model with the parameters BSA, blood aldosterone, and smoking, give an adjusted R-squared of 0.14 with a p-value of 0.01. For the analysis the data from the HERA 1, 2 and 3 study were used. During the first two HERA studies, mostly patients without renovascular disease were included. The baseline table showed that the clinical data and RFR measurements of the subjects without renovascular disease and the subjects with renovascular disease were comparable. The average RFR found in the overall HERA population was 2.11, which is in line with an earlier published study by Manoharan in 2006 (52).

The parameters kidney volume and renogram function division were only present in 8 and 13 patients respectively. Adding these parameters to a multivariate regression model is therefore not viable. Nonetheless, these parameters seem to have no added value in the determination of RFR, since these parameters are highly correlated to kidney length. The kidney length measurements can be easily performed using a CT, MRI or ultrasound scan, one of which is often available for patients with renovascular disease. Therefore, it is not recommended to gather kidney volume and renogram parameters outside the clinical routine in further research on this topic.

The added value of the RFR in the prediction of clinical response to PTRA has not been established yet. Invasive measurements are currently the only method of measuring RFR, but due to the invasive character and unfamiliarity of interventionalists with this procedure it is time-consuming to create patient databases with this method. A non-invasive method to determine RFR could help create a larger database in a shorter period of time.

Besides using clinical parameters to assess RFR non-invasively, other non-invasive options can be explored. First of all, as a part of the HERA 3 study, an attempt is made to estimate RFR based on GFR/ERPF measurements after a continuous low-dose dopamine infusion (3). Ongoing research should reveal whether this estimate correlates with the invasive measurement. In a study by Päivärinta et al. RFR-values in healthy and RAS patients were determined using oxygen-15-labeled water PET and with intravenous enalapril as a vasodilatant (44). In this study, no significant difference in RFR was found between healthy and stenosed patients. The study also did not compare the acquired values with intrarenal measured RFR-values, so the reliability of the measurements is still unknown. A measure which could be correlated to RFR, and might be easier to obtain, is the renal functional reserve. The renal functional reserve is a measure for the capacity of the kidney to respond to physiological demands, and can be measured by the increase in GFR after a protein-rich meal (53, 54). The renal functional reserve resolves the need for an invasive dopamine infusion, however, the increase in GFR cannot directly be translated into an increase in flow. Whether a correlation is present between the two measures needs further explorations. Doppler ultrasound, as can be used in assessment of coronary flow (55), might be used in the assessment of renal flow. The main issue however, is the need for an intrarenal bolus of dopamine to induce hyperaemia, the replacement of an intrarenal bolus with a systemically administered bolus needs further exploration.

2.5 Conclusion

Due to the limited number of patients included in the study, the power of the statistical analysis is low and it is precarious to draw conclusions. However, the statistical analysis presented in this chapter suggests that the RFR is a measure that presumably cannot be replaced by the already existing and frequently used parameters to quantify kidney value. Therefore, the invasive measurements of the RFR might be able to provide new information about kidney microvasculature status and be of added value in the prediction of clinical success of PTRA and potentially as a useful input for the CFD model. The development of an non-invasive measure to determine RFR could expedite research on appropriate patient selection for PTRA in the future.

3

Sensitivity analysis CFD-model

3.1 Introduction

The measures rFFR and translesional pressure gradient provide information on the pressure drop caused by the stenosis. CFD modelling is a non-invasive method to determine these values using numerical analysis. The determination of the rFFR and the pressure gradient in a stenosed renal artery using CFD has not been explored so far. In this chapter, the effect of several input values for the CFD model on the outcome measures rFFR and pressure gradient will be examined. Furthermore choices made for the settings used in chapters 4 and 5 are determined based on the results of this chapter.

3.2 Method

The different steps needed to perform a CFD simulation were explored in this chapter. In the following sections the different steps and the explorations performed are explained.

Geometry

The different methods of segmentation described in the background were explored. The arteries of interest are in our case the aortic artery, the affected renal artery and, if available, the contralateral renal artery and the superior mesenteric artery, given its proximity to the origin of the renal arteries. The 3D segmentation method was considered the most convenient method and was used for the further segmentations. SimVascular provides 3D segmentation tools from the Medical Imaging Interaction Toolkit (MITK). Due to practical limitations of the SimVascular toolkit, an external program was used for the segmentation process. 3D slicer is a free and opensource platform to perform 3D segmentations (50). The created model could be uploaded to the SimVascular environment and the model was smoothed

using a laplacian and constrain smoothing filter. The ends were trimmed, and the caps were assigned accordingly. Explorations were also performed on the level set method provided by SimVascular. However, the achieved models using this method where not representative for geometry of the arteries. For the simulations performed in this chapter a geometric model was created using a CTA scan from a patient from the Aarhus Medical Centre. All simulations were performed on the same geometric model. The steps needed in the segmentation proces and the final geometric model used in the analysis of this chapter can be seen in figure 3.1.

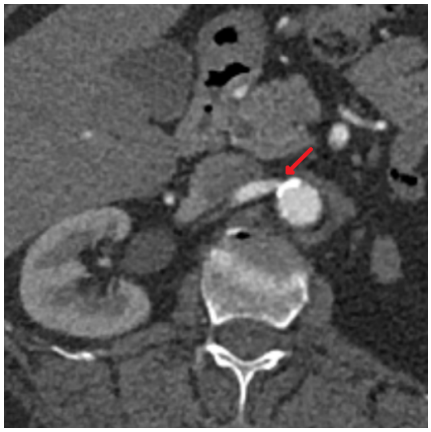

(a) CT image of a patient with RAS, indicated by the arrow.

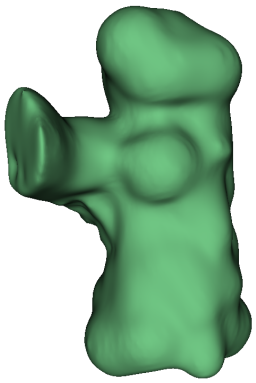

(b) Masking of the geometry of interest.

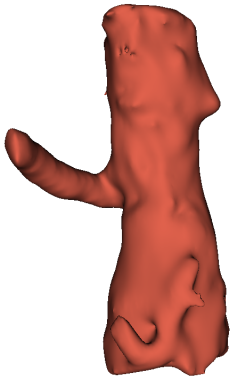

(c) Geometric model after threshold segmentation is applied.

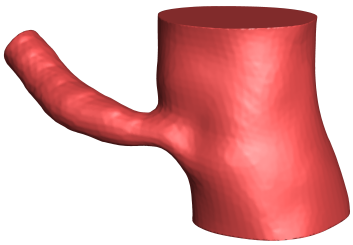

(d) Final geometric model after manual adaptation, smoothing and trimmed ends.

Figure 3.1: Geometric modelling using the 3D threshold method in 3D slicer

Meshing

Mesh convergence studies aim to find the smallness of the elements, specified by the global max edge size in SimVascular, needed to ensure that the simulation results do not change considerably by decreasing the size of the mesh. In the current study a mesh convergence study was performed using the model as shown in the previous paragraph. Global edge size started at 2, and a boundary layer of 3 layers was included in each model. Subsequently the global edge size was adapted in such a manner that the number of elements doubled. Accordingly, time step size should be altered in order to keep the temporal and spatial discretizations balanced. Simulations were performed using the different meshes to see how significantly the results changed for a finer mesh. As an output value, rFFR and pressure gradient were taken. The current study focuses on pressure values, and the necessity of the boundary layer in these simulations was unknown. The boundary layer however caused meshing problems due to intersecting facets, so scrapping the boundary layer would be convenient. Therefore the simulation results of meshes created without boundary layer, and meshes created with boundary layer were compared. Simulations using radius based meshing were compared to simulations without radius based meshing. The meshes all included a boundary layer made up of 4 layers.

Boundary conditions

The boundary conditions were determined to represent an average patient. Walls were simulated as rigid. As an inlet a distal pressure value was assigned of 98 mmHg (56). At the outlets a resistance value was applied. For the aortic outlet, the resistance was chosen corresponding to a flow rate through the cap of 1.9 L/min. For the renal artery the resistance was set in order to achieve a flow rate of 0.4 L/min. The flow rate values of these simulation were based on an article by Tayler et al. (57). Since the renal artery was slightly stenosed, the achieved flow rate trough the renal artery was 0.387 L/min. Both the pressure inlet, as well as the resistance value of the renal artery were altered in the current study.

Renal artery flow rate

The flow rate through the renal artery can easily be adapted by altering the resistance value. Alterations were made in the range of physiologically realistic flow rate values. Firstly the flow rate was altered in small steps of 10 percent, so that ultimatly flow rates ranging from 0.313 to 0.458 L/min were simulated. These simulations were used to examine the sensitivity of rFFR and aortic pressure - distal pressure (Pa-Pd) to a small alteration in the renal artery flow rate. Then the flow rate was altered more extremely, making the simulations range from 0.387 to 1.425 L/min.

Aortic pressure

The aortic pressure applied at the inlet increases the flow rate through the renal artery if the resistances are kept constant. In the current study, the renal artery resistance was altered in order to keep the flow rate through the renal artery constant.

3.3 Results

Meshing

The results of the mesh convergence studies are shown in figures 3.2 and 3.3. The simulation results achieved using boundary layer and radius based meshing with the most elements was assumed to be the true value. Errors were calculated relative to these values. As the number of elements increases the error tends toward zero. The mesh converges faster when using radius based meshing. Boundary layer meshing also lead to slower convergence, and a small error keeps existing in the simulation with the finest mesh without the boundary layer.

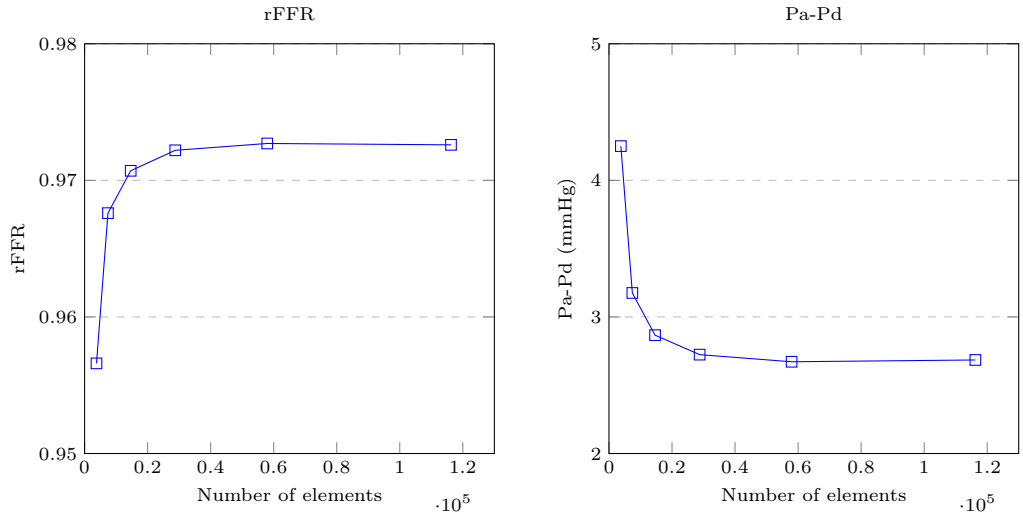

Figure 3.2: Mesh convergence plot for rFFR and pressure gradient

Flow rate

The sensitivity of rFFR and pressure gradient to a change in flow rate was tested using the simulations with small changes. An increase in flow rate through the affected renal artery led to a decrease in rFFR and an increase in pressure gradient. A change of 1 L/min increase in renal artery flow rate, led to a decrease of 0.16 in rFFR and an increase of 16 mmHg in pressure gradient. This corresponds to a change of 1.6e-04 and 1.6e-02 mmHg per mL/min

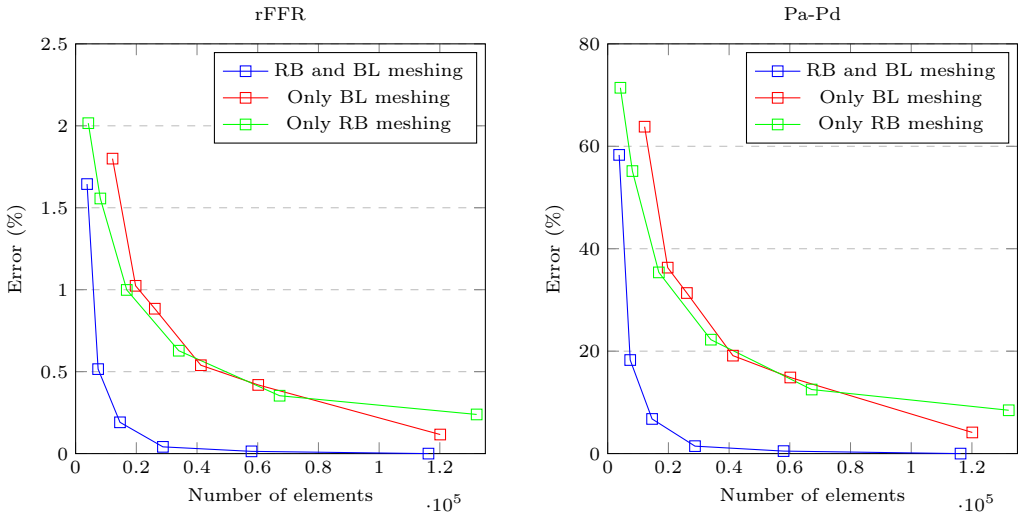

Figure 3.3: Errors of simulations performed with and without boundary layer (BL) and with and without radius based meshing (RB)

flow rate change respectively. In the graphs in figure 3.4 the results of alternating the flow rates more strongly are depicted. As can be seen, the relations are nonlinear.

Pressure

In figure 3.5 the results of alternating the aortic pressure are depicted. The resistance value is adjusted in order to keep the flow rate through the renal artery constant. As can be seen there is a linear increasing relation between distal renal artery pressure and aortic pressure. The rFFR also increases for larger aortic pressures, and the pressure gradient remains the same.

3.4 Discussion

Explain results

Mesh convergence

The results of the mesh convergence study showed the approximation of zero change when increasing the number of elements. The clinical relevance of change in rFFR is still topic of research, but current literature suggests that a systolic pressure gradient of at least 20 mmHg, and an rFFR cut-off point of 0.9 is clinically significant (32, 33, 58). Therefore a distal pressure change of 1 mmHg is considered to be an insignificant difference, which is roughly equivalent to a change of 1-2 percent in Pd. The corresponding change in rFFR is nearly equal to the change in Pd, since the imposed aortic pressure hardly changes in

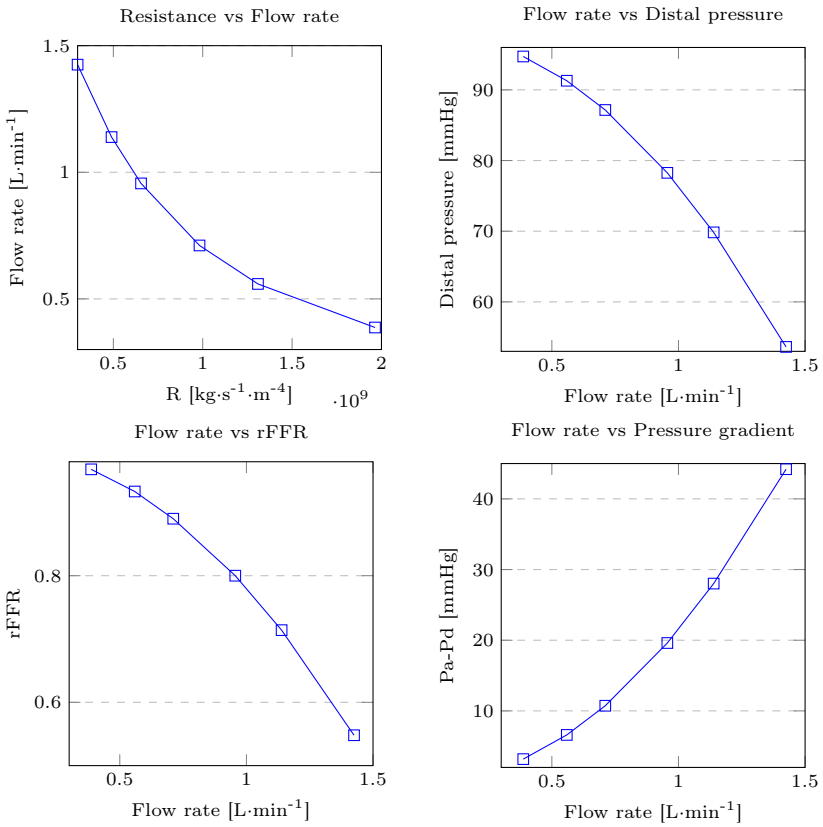

Figure 3.4: Influence of altering the renal artery cap resistance on flow rate, distal renal artery pressure, rFFR and pressure gradient (Pa-Pd)

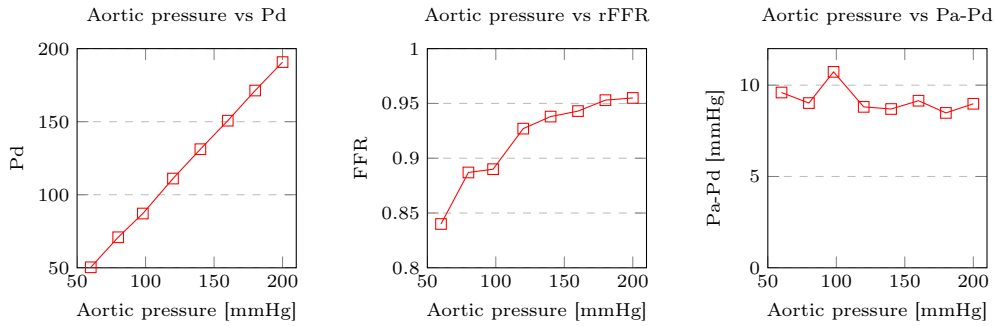

Figure 3.5: Influence of altering the aortic pressure while keeping renal flow rate constant.

consecutive simulations. The percentage change of the pressure gradient is more substantial than the change in rFFR, and it therefore takes longer to approximate the 0 percent change between consecutive meshes. This can easily be explained by the way the measures are calculated. Assuming an aortic pressure of 100 mmHg and a distal pressure of 80 mmHg the pressure gradient would be 20 mmHg and the rFFR 0.8. A change of 1 mmHg changes the pressure gradient by 5 percent, but the rFFR only changes by 1.25 percent. For larger rFFR's and therefore smaller pressure drops, this effect becomes more significant. Therefore, a larger percentage change is accepted for the pressure gradient. In the following chapters, the simulations will be performed on two different meshes of which the number of elements is doubled. If the change in Pd stays below the aforementioned percentages, the discretization error is considered to be small enough and the results are accepted. If the change is too substantial another simulation is performed using a finer mesh. This process will be repeated until a acceptable simulation is achieved.

The results in figure 3.3 show that both the boundary layer, and radius based meshing are good additions in the meshing process. Boundary layer meshing improves the solution, and radius based meshing helps to reduce computational time. Therefore the future simulations will be meshed with boundary layer and by radius based meshing.

Flow rate
From the simulations with the altered renal resistance, it is confirmed that an increase in flow rate causes a decrease in distal pressure. Since the aortic pressure applied in these simulations was kept constant, the rFFR decreases and the pressure gradient increases for higher flow rates. As explained in a paper by Young in 1979 (59), pressure drop over a stenosis is influenced by multiple factors. The dimensionless Reynolds number (Re) is used to determine whether fluid flow is laminar or turbulent. The number represents the ratio between inertial to viscous forces and is dependent on the viscosity, density, radius of the tube and velocity of the fluid. Fluid is mostly turbulent when Re exceeds $\backsim$ 3000, which can occur when a local decrease in vessel diameter causes a local increase in velocity. (15) For low Reynolds numbers, the pressure losses due to viscosity are dominant in flow and the relation between pressure drop and flow rate is linear. The viscous loss is given by Poisuille's Law where: $F = \frac{P_1 - P_2}{R}$ and R is dependent on the viscosity, length and radius of the tube. However, in complex geometries such as stenosis, an increase in velocity may lead to more turbulent flow due to the sudden expansion of the fluid. The loss of pressure due to inertial effects becomes more dominant. For higher Reynolds numbers the relation between flow rate and pressure drop that is present becomes quadratic. The flow-pressure relation observed in the simulations performed in this chapter have both linear as quadratic contributions, and the effective resistance of the stenosis increases for increasing flow rates. In our simulations,

the pressure gradient is the drop between Pa and Pd, the flow rate is the flow rate through the renal artery, and the resistance is the resistance caused by the stenosis. Due to the decreased renal cap resistance, flow rate through the renal artery increases leading to an increase in stenotic resistance. Therefore, an increase in pressure gradient has to follow. Since the aortic pressure was kept constant, the decrease in Pd goes along with a decrease in rFFR.

Pressure

In the simulations regarding the aortic pressure deviations can be seen that the pressure gradients stays roughly the same, but the rFFR increases for higher pressures. The renal artery resistance was adapted in the simulation such that the flow rate through the renal artery stayed the same, regardless of the implied aortic pressure. Since the flow rate, and therefore the stenotic resistance is kept constant, the pressure gradient has to stay constant as well. Therefore distal pressure should increase by the same number of mmHg as the aortic pressure. rFFR is defined as $\frac{Pd}{Pa}$ but can be rewritten as $1 - \frac{\Delta P}{Pa}$. This formula demonstrates that for increasing Pa and constant pressure gradient, the rFFR increases.

In the case that the aortic pressure would be increased, and the renal artery resistance would be kept the same, Pd would increase, rFFR would decrease and the pressure gradient would increase. At the cap of the renal artery Poiseuille's law can be applied, with the pressure gradient being the difference between Pd and venous pressure:

$$Pd = Q * R + Pv$$

Pv is assumed to be zero, and since the resistance is kept constant an increase in Pd goes along with an increase in renal artery flow rate, and visa versa. The increase in aortic pressure would therefore lead to an increase in both Pd and renal artery flow rate. The relative increase in Pd is smaller than the relative increase in Pa. The distal pressure is situated between the stenotic and cap resistance, and can therefore be calculated by:

$$Pd = Pa\left(\frac{R_{cap}}{R_{stenose} + R_{cap}}\right)$$

And subsequently:

$$rFFR = \frac{R_{cap}}{R_{stenose} + R_{cap}}$$

The stenotic resistance increases for increasing flow rates and therefore the relative increase in Pd becomes smaller for increasing aortic pressure, and thus rFFR decreases for increasing Pa.

Limitations and strengths

Geometry

Segmentation of the geometry is a time-consuming task prone to mistakes and very dependable on the user. The border between artery and surroundings is often difficult to determine,

especially around a stenosis due to calcifications and the small diameter of the vessel segment. The resolution of CTA images is limited, 1 mm per slice, and calcification results in blooming and partial volume artefacts, which might mistakenly amplify the appearance of calcification (60). A good educated approximation can be made about the course of the arteries, but however, the actual model will always slightly deviate from reality. The impact of deviations in the geometry has not been evaluated in the current thesis, but it is to be expected that the simulation outcomes are less accurate when mistakes in the geometry of the stenosis are used as input. A study on the uncertainty quantification in coronary blood flow simulations by Sankaran et al. showed that a uncertainty of the minimum lumen diameter of 0.6 mm in a idealized model with 60 percent stenosis leads to a change of 0.32 in coronary FFR. This uncertainty becomes larger for more severely stenosed arteries. Given the resolution of the CTA scans used in the current thesis, 1-2 mm, an error of 0.6 mm cannot be ruled out.

In a study by Mandaltsi et al. (61) rFFR values were determined in the renal arteries in a similar way. Their models were confined to the stenosed renal artery, yielding as an advantage an easier and shorter segmentation process. In their analysis, a comparison between models including and excluding aortic and contralateral renal segments was performed in two patients. Differences between Pd/Pa ratios acquired with the different models were small ($<$ 3.8 percent), although boundary layer conditions needed to be adjusted. It is worthwhile to explore the removal of different sections from the model and the effects on the simulation results in our data set.

Severity of stenosis in current chapter
In the current chapter the geometry of only one patient was used. The stenosis of this patient was mild, making the effects of varying different parameters on the outcome measures rFFR and Pa-Pd small. In more severly stenosed patients, the direction of the effect will remain the same, but the effect size will change. The quadratic effect of inertial energy loss is going to have an effect at lower flow rates. Besides, a finer mesh is needed to accurately simulate more severe stenosis.

Simulation supercomputer
To further strengthen the reliability of the simulations, in a later phase of this thesis, a simulation was performed with a very fine mesh and a simulation time and time step size much longer and smaller than the simulations performed in this thesis. For this simulation a computer with a high level of performance located in Amsterdam was used. The output results rFFR and Pa-Pd of this simulation were compared with a more coarse simulation as has been performed in this thesis. The deviations found were small (-0.22 percent for rFFR and 3.12 percent for Pa-Pd), indicating that the simulations as performed in the current

thesis are reliable for lesions of similary stenotic severity.

3.5 Conclusion

The segmentation of the geometery is time-consuming and difficult, but the most convenient method found for now is the method using external 3D slicer software. For the simulation of renal artery pressure, a converged simulation can be reached with a limited number of elements, which keeps computational time small. Radius based and boundary layer meshing methods are sensible additions to the meshing process, decreasing the computational time more. Flow rate through the renal artery affects both rFFR and Pa-Pd, whereas an increase in aortic pressure only affects the rFFR, and does not alter Pa-Pd.

4

Validation CFD-model

4.1 Introduction

CFD is a method to numerically evaluate arterial blood flow and the simulated results of the CFD algorithm is strongly dependent on the inputs of the model. The input values are often estimated, based on known averages, and are prone to deviations as described in the discussion of the previous chapter. Consequently, the output might deviate from reality. In this chapter, the rFFR and pressure gradient determined with CFD simulations are compared with the measured values from the HERA 3 study.

4.2 Method

The simulations performed in this chapter are all based on CTA images from the HERA 3 subjects. Subjects with successfully performed invasive measurements and high-resolution CTA scans were selected. Table 4.1 shows the patient characteristics. Geometries were created using the 3D segmentation method in 3D slicer and SimVascular as described in chapter 3. A total of 6 models have been created, which can be seen in figure 4.2. The models were meshed using the radius based meshing method. The global edge size was set at 1. An inward boundary layer was created using 2 boundary layers with a portion edge size of 0.5 and a layer decreasing ratio of 0.80. A second mesh was created using the same settings, except for the global edge size adjusted in such a manner that the number of elements doubled.

For all simulations, the blood viscosity was set at 4 centipoise and the density at 1.06 g/cm^3. Per patient, three simulations with different boundary conditions were performed. In simulations 1 and 2, average non-patient-specific values were used to set the boundaries. The

Table 4.1: Patient characteristic

Patient no	Age	Sex	Stenotic Side	Condition
2	49	Male	Right	FMD
6	42	Male	Left	FMD
8	65	Female	Right	ARAS
14	56	Male	Right	ARAS
16	76	Male	Bilateral (Measurements Right)	ARAS
19	71	Male	Right	ARAS

FMD = Fibromuscular dysplasia; ARAS = Atherosclerotic Renal Artery Stenosis

invasive measurements were used to set patient-specific boundary conditions in simulation 3. In simulation 1 an average pressure of 100 mmHg was set at the aortic inlet (62). At the aortic outlet, a steady flow rate of 1 L/min is imposed. Assuming a cardiac output of 5 L/min, this would imply the aortic outflow rate is 20 percent of cardiac output (63). The cap resistance was then calculated by the division of the aortic pressure by the targeted flow rate. For the contralateral renal artery and the superior mesenteric artery, if present in the model, a steady flow rate of 10 percent of cardiac output is assumed (63, 64). This implies a flow rate of 0.5 L/min through each artery, and the corresponding cap resistances were calculated. Any deviations from the targeted flow rate in the aortic, contralateral renal artery, and SMA outlets in the simulation results were not corrected by adjusting the cap resistances. It was assumed that deviations in flow rate through the arteries other than the affected renal artery do not meaningfully impact the rFFR and pressure gradient in the simulations. Steady flow rate through the affected renal artery was also assumed to be 0.5 L/min (63, 64). In chapter 3 was seen that the flow rate through the affected renal artery impacts the simulation results considerably, and therefore, imposing a realistic flow rate is important. The radius is an important and known indicator of the flow rate through a vessel. In a study by Taylor et al. in 2013 (10), flow rate through a stenosed coronary artery used for CFD simulations was determined using a relation in the form of Murray's law. Similarly, flow rate through the affected renal artery was adjusted. Literature suggests an exponent of 3 overestimates the relations between flow rate and radius, so it is suggested that the real values vary somewhere between 2 and 3 with a slight tendency towards 2 (65, 66, 67, 68). In this study, a value of 2.4 was used. It was assumed that the average renal artery flow rate of 0.5 L/min belonged to an average renal artery diameter of 5.5 mm (69, 70). The flow rate is then calculated by the following formula:

$$Q = 0.5 * \left(\frac{diameter}{5.5}\right)^{2.4}$$

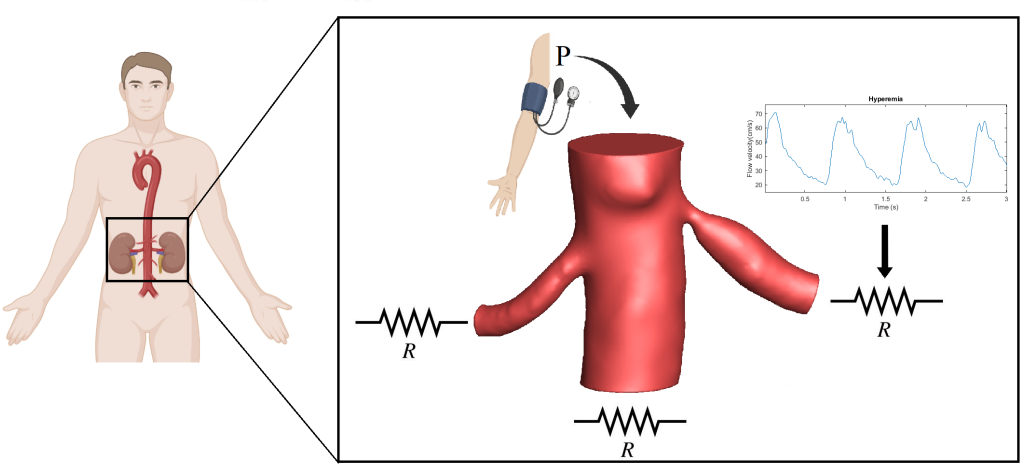

Figure 4.1: Geometric vascular model with RAS and the boundary conditions as applied in the current method.

The exact renal artery cap resistance needed to achieve the calculated flow rate was achieved by trial and error. In the second simulation, the calculated flow rate from simulation 1 was multiplied by 1.5 to achieve higher flow rates. In the third simulation, the measured aortic pressure was used as the inlet boundary condition. The invasively measured flow velocity profile during hyperaemia was converted to a flow rate using in-house Matlab scripts based on the presence of a Womersley flow profile, which is the analytical solution for fully developed pulsatile flow (71, 72). The achieved flow profile was averaged over time and used to determine the renal artery cap resistance at the outlet. The settings for the simulations used in this chapter can be seen in table 4.2

Simulations were performed until the correct flow value through the affected renal artery was achieved. The measure of the non-linear residual was aimed to be at most 1x10-3. Settings adjusted to improve the simulation results were the number of time steps, time step size, and the number of iterations within one step. Another simulation using a mesh with the number of elements doubled was then performed using the same inlet and outlet boundary conditions. Simulation settings were adjusted accordingly. If the change between the two meshes was considered to be small enough, as indicated in the discussion of chapter 3, the mesh was considered converged and the results were accepted.

Table 4.2: Simulation settings for the HERA 3 patients.

Patient	⊘ (mm)	Simulation 1	Simulation 2	Simulation 3	
		Flow rate (L/min)	Flow rate (L/min)	Flow rate (L/min)	Pa (mmHg)
2	5.6	0.52	0.78	0.28	99
6	6.8	0.83	1.25	0.55	107
8	2.8	0.10	0.15	0.21	123
14	5.8	0.57	0.85	0.58	119
16	3.4	0.16	0.24	0.10	135
19	5.5, 2.0	0.56	0.83	0.44	91

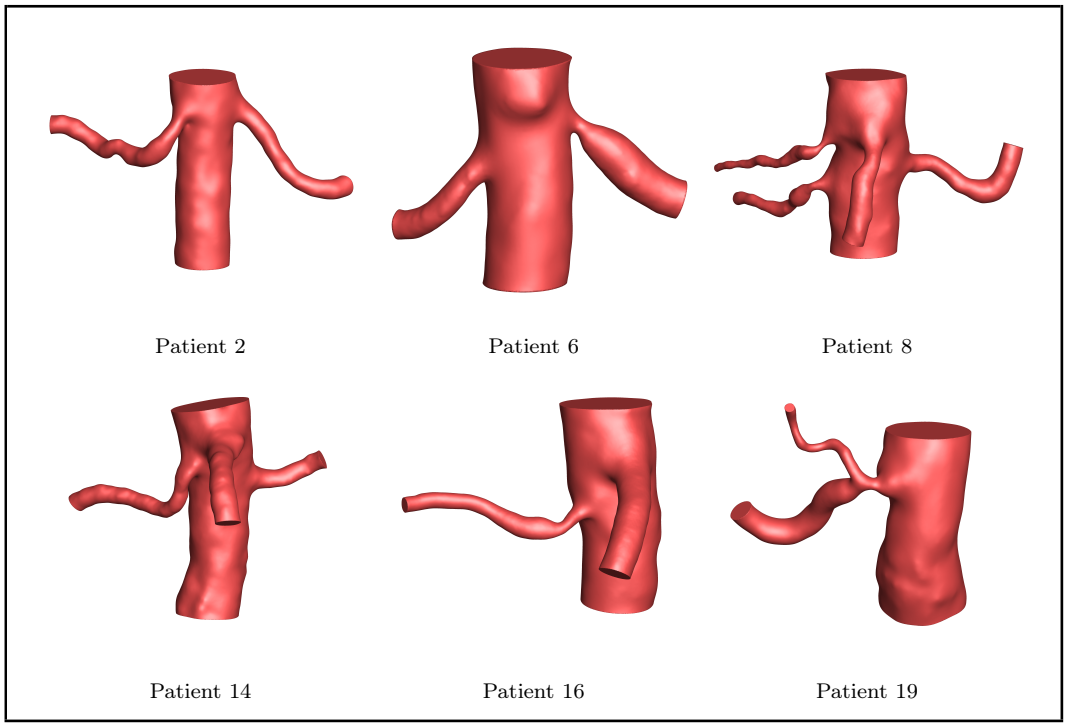

Figure 4.2: Geometries of the HERA3 patients

4.3 Results

A total of 3 simulations per HERA patient were performed. An example of a simulation performed on two of the patients can be seen in figure 4.3. For each simulation, the rFFR and the pressure gradient was calculated. The results of the simulations can be seen in table 4.3 alongside the measured values. In figure 4.4, the deviations per simulation from the measured values can be seen. HERA patient 8 was labelled an outlier since the results notably differ from the other patients, and was thus removed from calculations of the mean and standard deviations. The mean difference from the measured rFFR value for simulation 1 was -0.013 $\pm$ 0.028, for simulation 2 -0.180 $\pm$ 0.204 and for simulation 3 0.056 $\pm$ 0.067. For the pressure gradient these values were 1.11 $\pm$ 2.26, 17.63 $\pm$ 19.58 and -5.33 $\pm$ 6.84 respectively.

Table 4.3: Simulation results HERA3 patients.

Patient	Simulation 1		Simulation 2		Simulation 3		Measured	
	FFR	Pa-Pd	FFR	Pa-Pd	FFR	Pa-Pd	FFR	Pa-Pd
2	0.96	4.26	0.92	8.48	0.98	1.53	0.97	3.30
6	0.66	33.49	0.21	78.17	0.87	14.27	0.714	30.63
8	0.91	9.25	0.82	17.50	0.71	35.68	0.48	64.53
14	0.96	4.48	0.91	8.78	0.95	4.58	0.94	7.06
16	0.97	3.45	0.93	6.53	0.99	1.51	0.99	0.40
19	0.79	21.22	0.52	47.50	0.87	12.81	0.78	19.94

4.4 Discussion

In this chapter, CFD-simulations are used to non-invasively assess renal artery haemodynamics using solely routine CTA imaging as input. The results show that estimating rFFR and pressure gradient seems feasible, which in the future might lead to a diminished need for invasive renal haemodynamic measurements. The rFFR and pressure gradients of the three simulations were compared with the invasive measurements performed during angiography. The results show that simulation 1 matches the measured values the closest, with an average difference of -0.013 for rFFR and 1.11 for Pa-Pd. The imposed flow of 0.5 through the renal artery in simulation 1 is comparable to the average flow rate as seen in the HERA 3 data. In simulation 2 the flow imposed is probably too high, leading to the overestimation of the pressure drop caused by the stenosis. It was expected that simulation 3 would lead to the most accurate results, since the input values are based on the invasive measurements. The

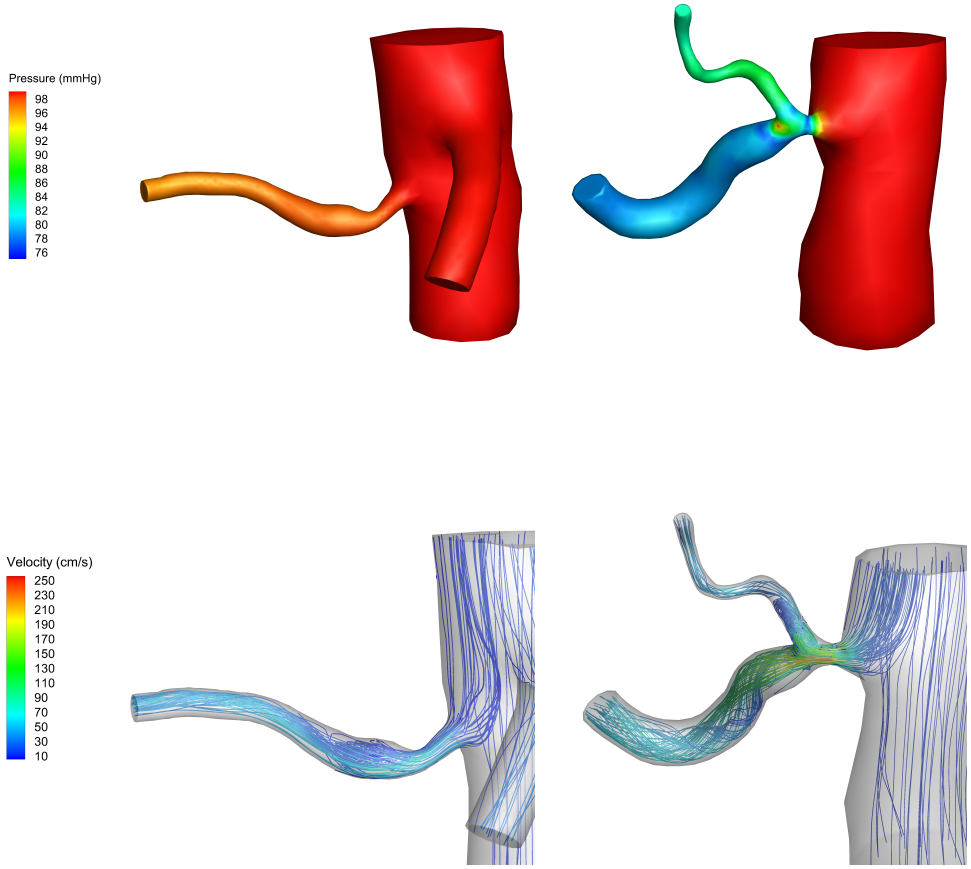

Figure 4.3: Examples from CFD simulation 1 in the HERA3 dataset. Pressure distribution (top row) and velocity streamtraces (bottom row) can be seen. Left: In-significant stenosis (rFFR = 0.97); Right: Significant stenosis (rFFR = 0.79).

observation that a standard flow corrected for vessel diameter provides more realistic results than imposing the measured flow during PTA raises questions about the reliability of the flow velocity measurements.

A recent study by Mandaltsi et al (2018) (61) compared Pd/Pa ratios derived by CFD with the invasively measured ratios in the resting state. Boundary conditions in this study were set based on general conditions of the renal vasculature in healthy people. The comparison between CFD-derived Pd/Pa ratios and measured ratios let to a mean difference of 0.015

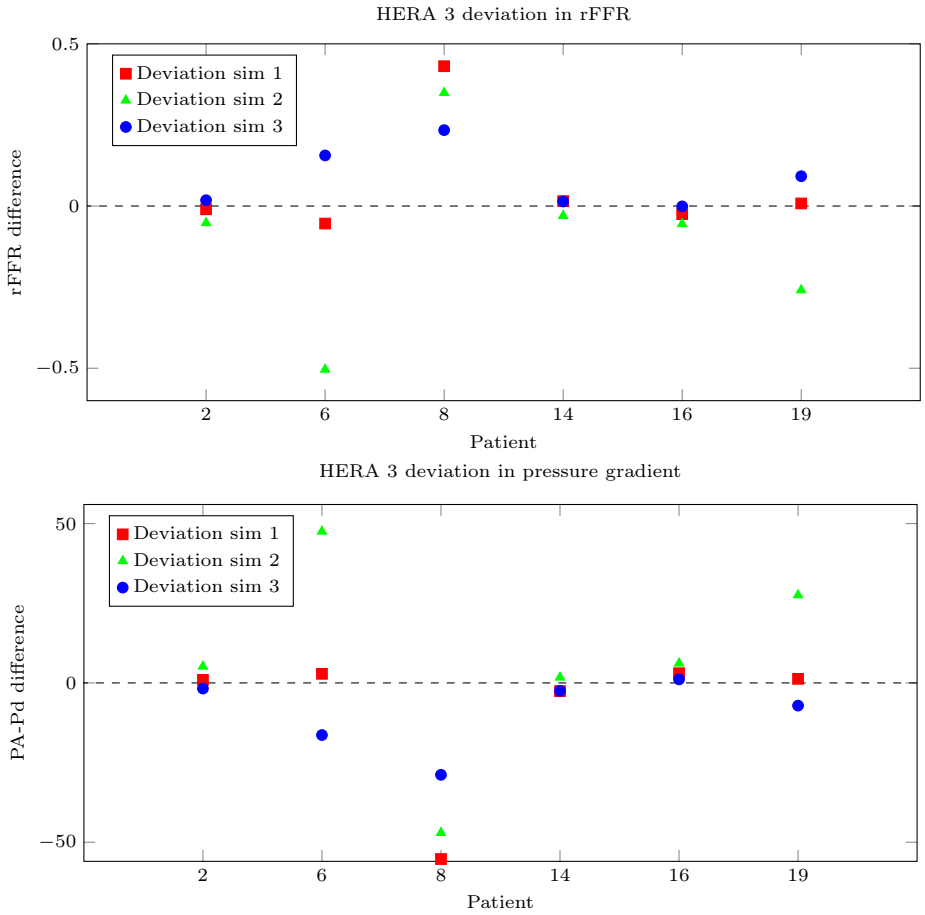

Figure 4.4: Deviations in simulated rFFR and pressure gradient from the invasively measured value.

which is comparable to the results acquired in our study. Mandaltsi et al. however focuses ratios acquired in the resting state, whereas the analysis presented here compares rFFR which is in the hyperaemic state, which is thought to be a better predictor of clinical outcome (33).

Outlier

The simulations of patient 8 deviates the most from the measured results and from the other patients and was thus labeled as an outlier. The pressure distribution from the different simulations can be seen in figure 4.5. Inspection of the angiographic images, showed that it was very likely that the catheter has been located in the stenosis during measurements. This results in a significantly reduced stenotic lumen, leading to the low rFFR and high pressure gradient measured. This measurement artefact was adjusted in the later HERA patients

included, the catheter was removed from the stenosis during the measurements.

Murray's law

According to Murray's law, there is a fixed relation between the vessel radius, and the volumetric flow rate through that vessel (73)(74). Murray's law assumes a minimal energy hypothesis, meaning that the costs of maintaining blood flow in any vessel is minimized. The two energy terms contributing to the total costs comprise the energy required to displace the fluid, which decreases when the vessel radius increases, and the metabolic energy for maintenance of the fluid, which increases for increasing vessel radius. According to Murray, an optimum arrangement is achieved for every vessel segment which led to the following equation:

$$Q = kD^3$$

Here Q is the volumetric flow rate through the vessel segment, D is the corresponding diameter, and k is a proportionality constant. The validity of Murray's law and the value of the exponent has been under discussion over the years (75). Several studies aimed to find the exact form of this relation, usually retrieving exponents around 2-3 (65, 66, 67, 68). The cubed law as proposed by Murray is based on the assumption of constant wall shear stress over the whole arterial system. In vivo measurements by Reneman et al. (2008) (67), however, showed that WSS varies over the arterial tree. The authors suggest an exponent varying from 2 in large arteries near the heart to 3 in arterioles. No consensus has been found about the relationship between flow and radius in the renal arteries. The value of 2.4 chosen for the current study is based on the knowledge retrieved from the studies described above and is in line with the non-Newtonial model introduced by Revellin et al. in 2009 (66).

The consequence of this value is that vessels with a large radius have a much larger flow imposed than vessels with a smaller radius. Whereas it is expected that this is in line with reality for healthy arteries, it is unknown how this relation exists in stenosed arteries. Blood vessels modulate size as a response to a change in flow and altered wall shear stress sensed by the endothelial cells (76). Processes typically occurring within 4 to 6 weeks (77). It is our hypothesis that the renal arteries adjust to the decreased flow caused by the stenosis, by decreasing it's radius. The time course of renal artery modulation after stenosis is not clear, which makes it difficult to determine how to relate form and function in stenosed arteries. Additionally, the data analysed in the current thesis contained a number patients with a seemingly inflated renal artery after the stenosis compared to the contralateral renal artery. Arterial wall damage induced by turbulence caused by the stenosis might lead to post-stenotic dilatation (78), which would plead against the use of our hypothesis of decreasing radius. Furthermore, the results of chapter 3 showed no significant relation between the measured flow velocity and renal artery diameter. Imposing no relation between radius and

flow would be unrealistic, but imposing the wrong relation might have consequences too. If the value of 2.4 is chosen to high, it would lead to excessively high imposed flow values in the renal arteries with a larger radius, which in turn leads to a lower rFFR as seen in chapter 3. The flow imposed in the arteries with a small radius on the other hand might be too small, thereby underestimating the severity of the stenosis.

CFD limitations
In the current simulations only steady flow was simulated. Adding pulsatile flow to the CFD model could lead to a change in the rFFR and pressure gradient results. It is however expected that this change would be minor.

4.5 Conclusion

The data set used for the comparison is small, so caution is needed when drawing conclusions. However, these initial results are hopeful, showing that the measured rFFR and pressure gradient can be well approximated by a CFD simulation, despite not knowing the flow rate. The remaining patients included in the HERA 3 study can be added to the analysis to increase the power of the results.

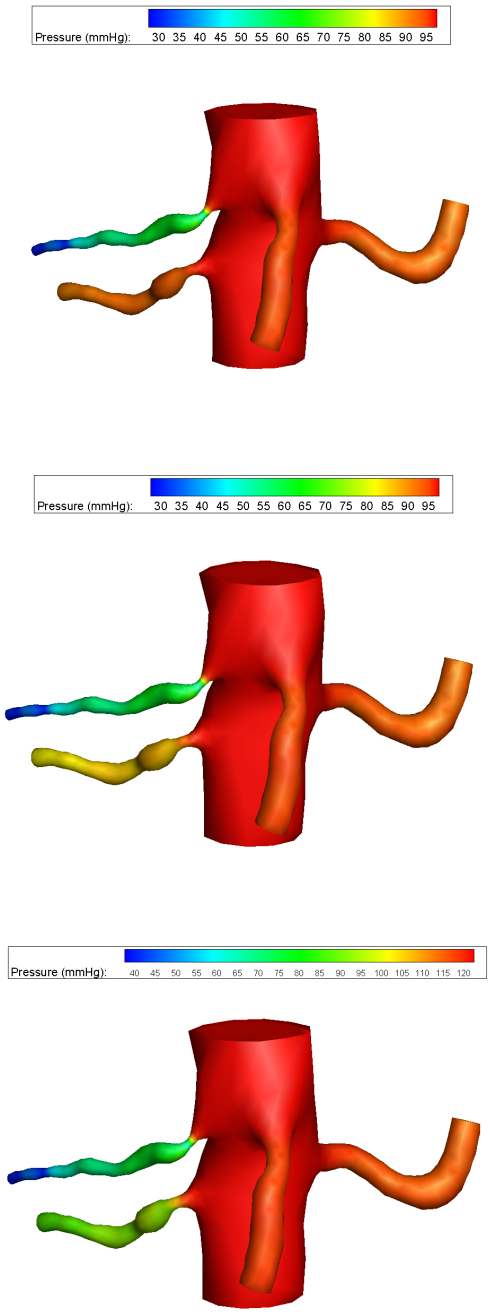

Figure 4.5: Pressure distributions acquired from simulation 1 (top row), simulation 2 (middle row) and simulation 3 (bottom row) of patient 8.

5

CFD-model application

5.1 Introduction

The clinical purpose of the ongoing research is to determine the benefits of PTRA on blood pressure and kidney function prior to angioplasty. Based on solely the anatomical grading, it is difficult to determine the functional impact of the stenosis (79, 80). With the use of CFD, additional information about the effect of the stenosis on the velocity and pressure profiles can be obtained. The rFFR and pressure gradient can be derived from the CFD solution. Clinical data from a prospective cohort of patients treated for RAS from the Aarhus University Hospital were made available for analysis (81). The aim of this chapter is to provide insights into the predictive value of CFD simulations in patients undergoing PTRA.

5.2 Method

From the Aarhus University Hospital, a data set of patients who underwent PTRA is made available for this analysis. All subjects had a CTA scan and had their eGFR and mean 24-hour ambulatory systolic blood pressure monitored for an average of 2 years. From the database, a total of 11 patients were selected, of which one patient had a bilateral RAS, with a stenosis of approximately 50-80 percent. Patients were aged between 48 and 81, including both males and females. Follow-up data on systolic blood pressure change, change in defined daily dose and change in eGFR after 12 months were available. Systolic blood pressure was corrected for change in defined daily dose by 8 mmHg as suggested by the Aarhus hospital, which is in line with literature (82). The geometries of the arteries can be seen in figure 5.1. Simulations 1 and 2 were performed in the same manner as simulations 1 and 2 from the previous chapter, and the rFFR and pressure gradients were determined for

each patient. Patient 44 was treated on a bilateral stenosis. However, since it is expected that the most significant stenosis has the largest impact on clinical outcome, the stenosis on the most severe side was taken for analysis. During the whole segmentation and simulation process, the outcome of the intervention was blinded to the researchers in the Amsterdam UMC. After obtaining all the simulation results, the rFFR and translesional pressure gradients were compared with the clinical outcome of the intervention.

Table 5.1: Patient characteristic

Patient no.	Age	Sex	Stenotic Side	No. of functional kidneys	BP	DDD	eGFR
3	70	Female	Right	1	181	5.58	23
10	62	Female	Right	2	170	9.33	16
19	48	Female	Right	2	176	4.33	103
29	81	Female	Left	1	181	12.67	10
31	78	Male	Left	2	153	3.42	42
36	73	Female	Left	1	153	3.67	27
44	64	Male	Bilateral	2	160	4.33	90
56	62	Female	Left	1	152	8	70
57	76	Male	Left	1	161	3.33	27
63	77	Female	Right	1	195	8	29
115	63	Male	Right	2	194	5	76

BP = Blood pressure at baseline; eGFR = Estimated glomerular filtration rate at baseline; DDD = Defined daily dose at baseline.

5.3 Results

The rFFR and pressure gradients achieved from the CFD-simulations in the Aarhus data set can be seen in table 5.2, with the corresponding artery diameters and flow rates implied. Assuming the critical rFFR value of 0.9 or a pressure gradient of 10 mmHg, simulation 1 indicated 5 patient with significant, and 6 patients with insignificant stenosis. An example of a significant and insignificant simulated stenosis can be seen in figure 5.2. In figures 5.3 and 5.4 the simulation results of simulation 1 are plotted against the clinical outcomes of PTRA regarding systolic blood pressure change with and without correction for change in defined daily dose. Four out of five patients with significant stenosis showed a decrease of >10 mmHg in systolic blood pressure after PTRA, opposed to two out of six patient with insignificant stenosis. After correction for change in defined daily dose, four out of six patients with insignificant stenosis showed a clinical significant decrease in systolic blood presssure. A total of five patients had a decrease in eGFR at baseline of >5 ml/min. Four out of those five patients had a simulated rFFR of ≤ 0.9, of which eGFR in three patients

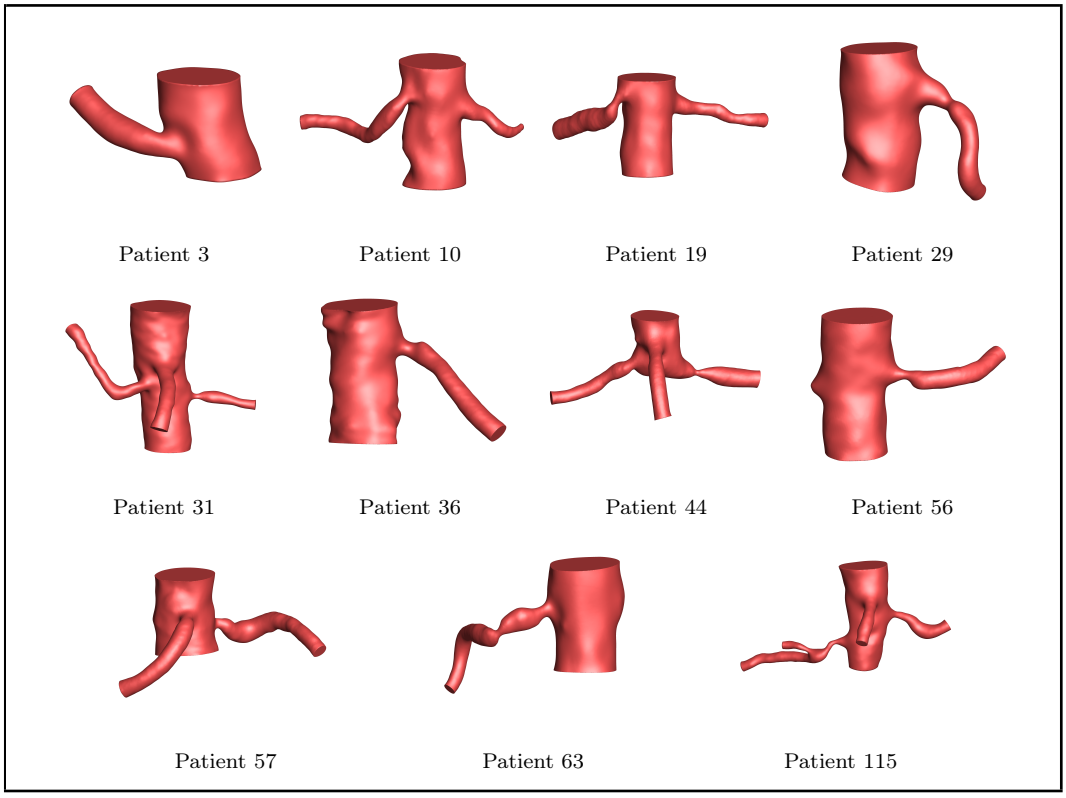

Figure 5.1: Geometries of the Aarhus patients

stabilised after PTRA. In one patient with and one patient without significant stenosis and decrease in eGFR at baseline of >5 ml/min, eGFR worsened after PTRA. Simulation 2 showed similar results to simulation 1, except that the differences in simulation outcomes between patients were magnified.

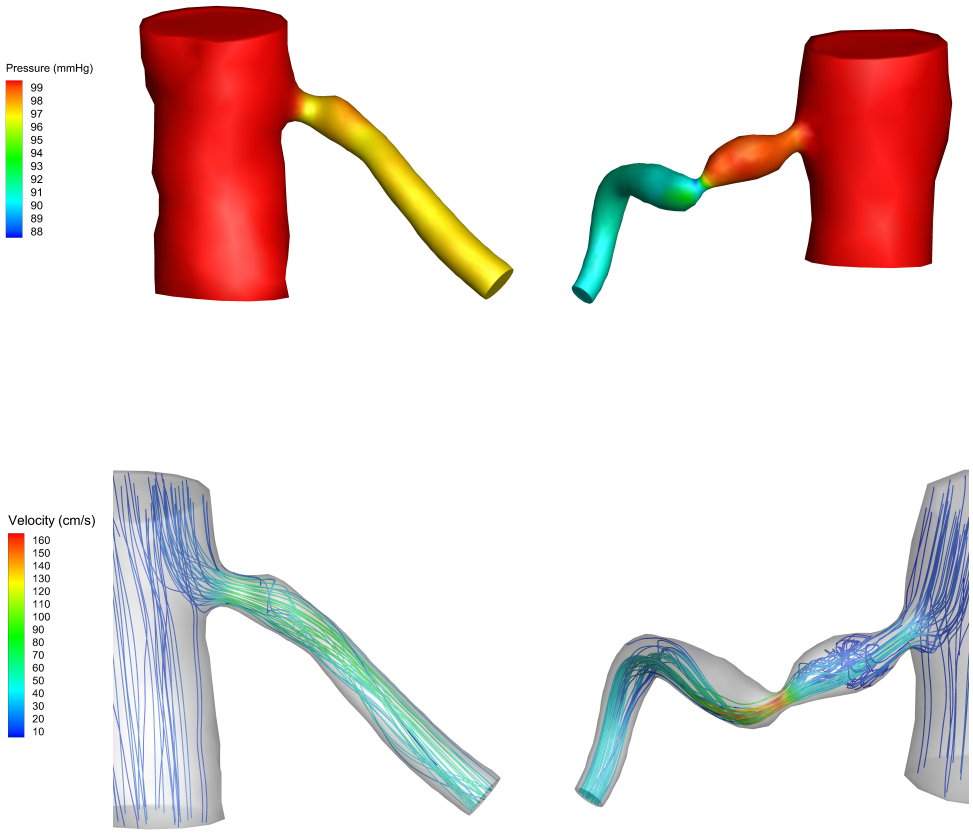

Figure 5.2: Examples from CFD simulations in the Aarhus dataset. Pressure distribution (top row) and velocity streamtraces (bottom row) can be seen. Left: In-significant stenosis (rFFR = 0.97); Right: Significant stenosis (rFFR = 0.90).

5.4 Discussion

The predictive value of simulated renal artery pressures on clinical benefits such as blood pressure decline and eGFR increase is evaluated in this chapter. The results must be inter-

Table 5.2: Simulation results Aarhus patients.

Patient no.	⊘ (mm)	Simulation 1			Simulation 2		
		Flow rate (L/min)	rFFR	Pa-Pd	Flow rate (L/min)	rFFR	Pa-Pd
3	6.3	0.68	0.97	3.11	1.03	0.93	7.43
10	3.6	0.18	0.98	1.99	0.27	0.96	3.85
19	6.4	0.71	0.79	20.51	1.07	0.52	47.48
29	3.5	0.17	0.98	1.70	0.26	0.96	3.50
31	3.9	0.22	0.90	10.46	0.33	0.76	24.27
36	5.7	0.41	0.97	2.93	0.62	0.94	6.03
44 Left	3.0, 3.0, 3.4	0.39	0.83	16.69	0.59	0.59	41.03
44 Right	5.3	0.46	0.97	2.96	0.69	0.94	6.11
56	5.0	0.40	0.93	6.60	0.60	0.83	16.86
57	5.2	0.48	0.92	7.93	0.66	0.81	19.01
63	3.4	0.16	0.90	9.52	0.24	0.81	18.94
115	4.9, 3.6	0.56	0.74	25.71	0.84	0.46	54.18

⊘ = Renal artery diameter; Flow rates imposed in simulation based on diameter.

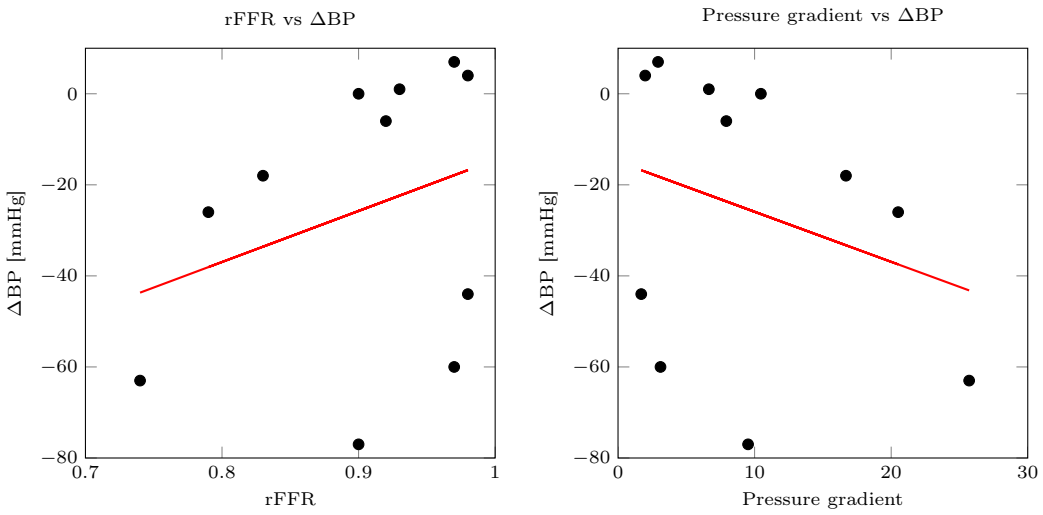

Figure 5.3: Simulated rFFR and pressure gradient of simulation 1 plotted against the change in systolic blood pressure (ΔBP) after PTRA.

preted with caution due to the limited number of patients. The results in figure 5.3 suggest there is a weak correlation between simulated significance of the stenosis and systolic blood pressure outcome. However, when corrected for defined daily dose, this relation cannot be seen anymore, see figure 5.4. Most patients with a simulated significant stenosis responded with good clinical outcome, both in systolic blood pressure change as in eGFR change. The results showed that some patients with a simulated insignificant stenosis still showed a good

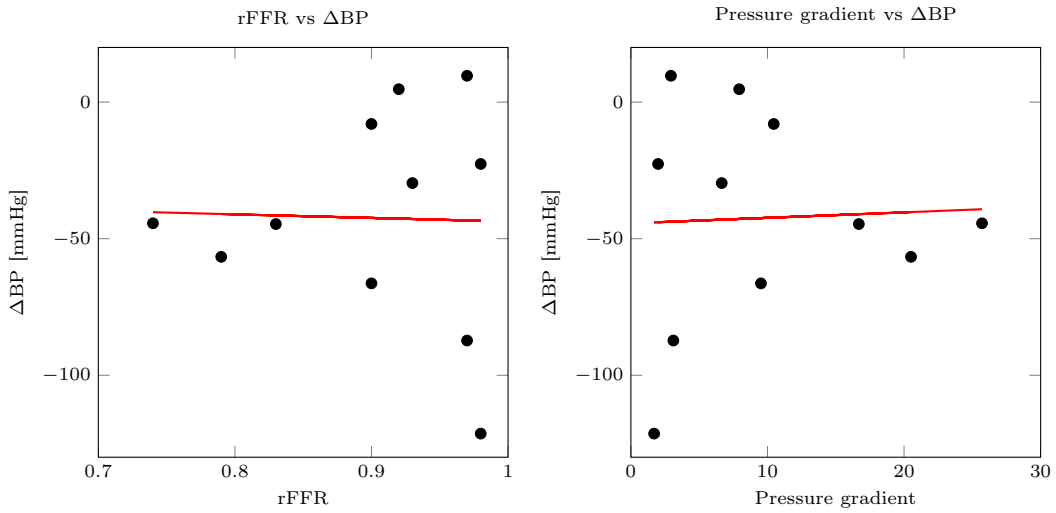

Figure 5.4: Simulated rFFR and pressure gradient of simulation 1 plotted against the change in systolic blood pressure (ΔBP) corrected for change in defined daily dose after PTRA.

response in systolic blood pressure, with and without correction. One patient with significant stenosis did not respond.

A possible explanation to the good response in blood pressure despite insignificant stenosis can be an increased adherence of the patients due to the invasive treatment. Use of medication might be improved, and health style might be adapted as response to an invasive intervention. Another thing that should be mentioned is that patients 10 and 56 did not show a decrease in systolic blood pressure, but did show a decrease in defined daily dose. However, their baseline systolic blood pressures were respectively 170 and 152. The corrected blood pressure decline suggests a good response to the treatment. However, the question rises whether the physicians decision to reduce defined daily dose can be related to the intervention. It may be that poor compliance with therapy of these patients is the rationale for the physicians decision. It would be expected that decrease in defined daily dose due to the intervention would be in the case of a healthy blood pressure, whereas these patients still have severe hypertension.

Another possible explanation for the unexpected response in some patients can be that the CFD simulation method described in the previous sections might not be accurate enough in determining the stenotic significance. The CFD limitations described in the previous chapters also apply here. As touched upon in the discussion of chapter 3, deviations in the

geometry lead to considerable errors in the simulated renal artery pressure. The CTA scans used to create the geometry in Chapter 4 had a higher resolution than the CTA scans used for this chapter, a slice thickness of 1 and 2 mm, respectively. This presumably led to larger errors in the segmentation of the Aarhus patients, making the simulation results less reliable.

The simulated results only provide information on the significance of the stenosis. Renal microvasculature is not taken into account, and could not be predicted based on the clinical parameters as described in chapter 2. The significance of the stenosis on itself can be determined using CFD simulations, but might not provide sufficient information about the benefits of removing the stenosis. The wrong predictions on outcome measurements done based on the rFFR and Pa-Pd in this chapter may be due to the lack of this information. The expectation is that to make a good estimation of the benefits provided for a patient, the combination between stenosis significance and microvasculature status is needed.

For each patient, a simulation with higher flows imposed was performed. The results showed that the rFFR and pressure gradients in simulation 2 were similar to simulation 1, except for the amplification of the differences between patients. Therefore, simulation 2 does not seem to add value to the interpretation of the results. The critical rFFR value of 0.9 was better able to distinguish between responders and non-responders in simulation 1 than in simulation 2. This encourages the preference for an averaged imposed flow value of 0.5, as in simulation 1, which was also supported by the findings in chapter 4.

5.5 Conclusion

The currently developed CFD methodology for the prediction of clinical outcome of PTA is not sufficient to accurately select the patients most likely to benefit. The aforementioned limitations of this chapter, in combination with the promising results of the previous chapter and the added predictive value of renal pressure measurements known from literature encourage further exploration of the application of CFD in renal vessels. Further studies should include more of the Aarhus patients in order to statistically asses the predictive value of simulated rFFR and pressure gradient. In the next chapter the future perspectives on this area of research will be elaborated.

6

Future perspectives

This thesis elaborated on the application of CFD simulations in the prediction of clinical response after PTRA in patients with RAS. The findings of chapter 4 encourage to explore the use of CFD-simulations to asses renal haemodynamics in a larger clinical database, within a clinically relevant range of rFFR and pressure gradients. First, the validation of the currently developed CFD model can be extended by including the remaining patients from the HERA 3 study. The external data set from Denmark included a total of 97 patients, of which only 11 patients were included in the current thesis. The results in chapter 5 showed a limited correlation between simulation results and blood pressure or kidney function improvement. A natural progression of this work is to analyse the current simulation settings on the entire data set to see if the expected correlations will become stronger and to statistically assess its predictive power. Furthermore it is recommended to assess whether the combination of simulated results with the predictive clinical parameters found by Reinhard et al. (81) could improve the prediction. The suggested relevant parameters found in this study were increasing 24-hour ambulatory systolic blood pressure at baseline, discontinuation of ACEi/ARB because of an increase of 30 percent in plasma creatinine and age for the prediction of blood pressure change. Female sex, 24-hour ambulatory systolic blood pressure at baseline, rapidly declining kidney function at baseline and recurrent heart failure or sudden pulmonary edema were the predictors for estimated GFR improvement after PTRA. Additional predictive parameters found in other studies, such as body mass index (BMI) (83), and other clinical parameters as described in a review by mishima et al. (84) could be considered.

The current CFD model can be further developed and expanded to include more patient-specific boundary conditions. Firstly, the segmentation of the geometry is time-consuming, is prone to error and very user dependent. The Level Set method addressed in chapter 3 could

in theory overcome the user dependency and time-consuming problem. Other developments in automated 3D segmentation algorithms are currently ongoing (85). A promising technique is to used deep learning algorithms for segmentation. Li et al. (86) created a deep learning algorithm for recognising coronary stenosis from CT angiography, which provides quick and accurate segmentation of the coronary arteries. However, low or mixed density plaques and sites with complex anatomy are still a challenge for artificial intelligence (86). An ongoing challenge is to find the most suitable method for stenosed renal artery segmentation which is complicated by the abnormal caliber around the stenosis and calcifications. Developments in the further future that could improve the model such as ultra-high-resolution CT, as proposed by Latina et al. (87) for evaluation of severely calcified coronary lesions, could contribute in creating a reliable geometry for CFD simulations. This development in CT technology has the advantage that artifacts from calcifications and stents are reduced.

Secondly the in- and outlets could be adjusted to a more patient-specific input. In the current thesis a population-averaged mean aortic pressure (MAP) was used to set the inlet aortic pressure. Blood pressure measurements could be used to estimate the MAP for each individual patient, although the results in chapter 3 showed that pressure gradient remained constant over various inlet pressures because the renal resistance was simultaneously compensated to maintain the targeted renal flow rate. The renal flow rate has a more important impact on simulation results. Currently, there is no reliable method to non-invasively estimate hyperaemic flow. The two hurdles to overcome here are the non-invasive measurement of renal artery flow, and achieving the hyperaemic state without intrarenal dopamine bolus. In addidtion, information on hyperaemic renal artery flow provides information on microvasculature which could contribute to the prediction of clinical outcome after PTRA. Renal Doppler ultrasound is a routinely used technique to measure renal artery blood flow (88). This technique is non-invasive, low-costs and convenient. However, doppler ultrasound is operator-dependent due to the complex and tortuous anatomy and sometimes unobtainable due to bowel obstruction. Renal artery Doppler Measurements are often available in patients with RAS, and therefore it would be interesting to see if hyperaemic renal artery flow can be estimated from these measurements. Contrast-enhanced ultrasound (CEUS) uses microbubble contrast agents to assess microvascular perfusion and renal artery flow (89, 90). In a study by Kalantrinia et al. (90) an increase in renal blood flow was induced by a high-protein meal and renal blood flow was measured by CEUS. Developments in phase contrast magnetic resonance imaging flow measurement (PC-MRI) makes is possible to asses renal artery flow more accurately (91, 92, 93). PC-MRI is however high-cost and less accessible compared to Doppler ultrasound (93). Estimating hyperaemic flow based on baseline measurements remains a challenge for these techniques. Low-dose dopamine infusion might be an alternative to the intrarenal dopamine bolus to induce hyperaemia and is being tested

in the HERA 3 study (3). CEUS measurements seem promising, since the measurements are convenient, patient friendly, relatively low-cost and ultrasound measurements are part of standard practise in RAS patients. Besides, measurements of the renal cortical thickness, which could also be acquired using ultrasound, could be an indicator of kidney function (94). Future studies on CEUS and ultrasound measurements to assess whether the aforementioned mentioned hurdles could be overcome is therefore recommended.

Application of CFD in clinical practise

This thesis focused on the application of CFD to eventually contribute in decision-making for renovascular treatment. For the application of CFD in clinical practice, the workflow needs to be standardised and automated. The current method to determine rFFR and pressure gradient using CFD is very time-consuming. As previously mentioned, a standardised method to obtain a geometric model should be developed. In addition, in the current thesis, getting to the right simulation setting was time-consuming since the resistance had to be altered in order to get the correct renal artery flow. For clinical applicability it is recommended to find a more straightforward and easy approach to set the boundary conditions. Perhaps the boundary conditions can be adjusted automatically based on the output of the simulation. The user has to indicate the desired flow or pressures, and the simulation loop can be repeated until these values are reached. With the improvement of computing resources, computation time will become shorter in the future. The Simvascular software used for the simulations in the current thesis has some limitations. The software can be unstable, causing the program to close down spontaneously, or slow down significantly at random moments. Crashes occurred during segmentation, face extraction, re-meshing and meshing steps. Errors during the process are not evident, and are currently solved by trial and error. However, it should be mentioned that the SimVascular solver is quite stable, opposed to other CFD solvers used for vascular simulations. In addition, SimVascular is an accessible program for beginners in the field and has the advantage that all steps of the process can be done in the same software. Still, software providing more stability and more information on the cause of the error would be needed if CFD is applied in clinical practise. Lastly, CFD technology should be properly used, calibrated, tested and interpreted to be of value in clinical practice. Sufficient knowledge on both the technical background of CFD and on the implications of the results on clinical practise is needed. A technical physician can bring the two disciplines together and is preeminently suited for this task.

7

Conclusion

The application of CFD in the renal arteries might be of great benefit in the selection of patients for PTRA in the future. The results provided in the current thesis demonstrate that CFD is suitable for the non-invasive assessment of renal haemodynamics. The validation study showed that rFFR and translesional pressure gradient could be estimated with an accuracy of -0.013 $\pm$ 0.028 and 1.11 $\pm$ 2.26 respectively. Application of the CFD model to assess clinically predictive value did not lead to the desired results, however, hope should not be abandoned given the size of the data set and the potential developments in the field. Future research should show whether the haemodynamic parameters are appropriate to improve patient selection, in which improved CFD models can accelerate the process.

Bibliography

[1] H. G. Rennke and B. M. Denker, *Renal pathophysiology*. Lippincott Williams & Wilkins, 2014.

[2] M. Prince, J. D. Tafur, and C. J. White, "When and How Should We Revascularize Patients With Atherosclerotic Renal Artery Stenosis?," 3 2019.

[3] B. v. d. Born, L. Vogt, and L. v. d. Velde, "Functional Renal Hemodynamics in Patients with Renal Artery Stenosis 3," tech. rep., Amsterdam University Medical Centers, 2019.

[4] L. van de Velde, D. Collard, W. Spiering, P. M. van Brussel, J. Versmissen, T. Wierema, M. W. de Haan, I. J. Zijlstra, A. A. Kroon, L. Vogt, P. W. de Leeuw, D. van Twist, and B. J. van den Born, "New diagnostic and treatment strategies in renal artery stenosis: A promising pursuit or disappointment foretold?," *Netherlands Journal of Medicine*, vol. 78, no. 5, pp. 232–238, 2020.

[5] S. M. Herrmann and S. C. Textor, "Renovascular Hypertension," *Endocrinology and Metabolism Clinics of North America*, vol. 48, no. 4, pp. 765–778, 2019.

[6] D. Lao, P. S. Parasher, K. C. Cho, and Y. Yeghiazarians, "Atherosclerotic renal artery stenosis - Diagnosis and treatment," *Mayo Clinic Proceedings*, vol. 86, no. 7, pp. 649–657, 2011.

[7] C. M. Cheung, J. Hegarty, and P. A. Kalra, "Dilemmas in the management of renal artery stenosis," *British Medical Bulletin*, vol. 73-74, pp. 35–55, 2005.

[8] D. Vassallo, J. Ritchie, D. Green, C. Chrysochou, and P. A. Kalra, "The effect of revascularization in patients with anatomically significant atherosclerotic renovascular disease presenting with high-risk clinical features," *Nephrology Dialysis Transplantation*, vol. 33, pp. 497–506, 3 2018.

[9] J. Ritchie, D. Green, C. Chrysochou, N. Chalmers, R. N. Foley, and P. A. Kalra, "High-risk clinical presentations in atherosclerotic renovascular disease: Prognosis and re-

sponse to renal artery revascularization," *American Journal of Kidney Diseases*, vol. 63, pp. 186–197, 2 2014.

[10] C. A. Taylor, T. A. Fonte, and J. K. Min, "Computational fluid dynamics applied to cardiac computed tomography for noninvasive quantification of fractional flow reserve: Scientific basis," *Journal of the American College of Cardiology*, vol. 61, no. 22, pp. 2233–2241, 2013.

[11] T. P. van de Hoef, F. Nolte, M. C. Rolandi, J. J. Piek, J. P. van den Wijngaard, J. A. Spaan, and M. Siebes, "Coronary pressure-flow relations as basis for the understanding of coronary physiology," *Journal of Molecular and Cellular Cardiology*, vol. 52, no. 4, pp. 786–793, 2012.

[12] D. U. Silverthorn, "Human Physiology: An Integrated Approach, Global Edition," in *Human Physiology: An Integrated Approach, Global Edition*, ch. The kidney, pp. 594–600, 2018.

[13] A. Denic, J. Mathew, L. O. Lerman, J. C. Lieske, J. J. Larson, M. P. Alexander, E. Poggio, R. J. Glassock, and A. D. Rule, "Single-Nephron Glomerular Filtration Rate in Healthy Adults," *New England Journal of Medicine*, vol. 376, pp. 2349–2357, 6 2017.

[14] P. E. Stevens and A. Levin, "Evaluation and Management of Chronic Kidney Disease: Synopsis of the Kidney Disease: Improving Global Outcomes 2012 Clinical Practice Guideline," 2013.

[15] W. F. Boron and E. L. Boulpaep, *Medical physiology.* Elsevier Saunders, 2012.

[16] A. M. R. Agur and A. F. Dalley, *Grant's Atlas of Anatomy.* 2013.

[17] P. T. Sawicki, S. Kaiser, L. Heinemann, H. Frenzel, and M. Berger, "Prevalence of renal artery stenosis in diabetes mellitus — an autopsy study," *Journal of Internal Medicine*, vol. 229, no. 6, pp. 489–492, 1991.

[18] H. Goldblatt, J. Lynch, R. F. Hanzal, and W. W. Summerville, "Studies on experimental hypertension: The production of persistent elevantion of systolic blood pressure by means of renal ischamia," 1934.

[19] P. Wiesel, L. Mazzolai, J. Nussberger, and T. Pedrazzini, "Two-Kidney, One Clip and One-Kidney, One Clip Hypertension in Mice," *Hypertension*, vol. 29, no. 4, pp. 1025–1030, 1997.

[20] K. Wheatly, N. Ives, P. A. Kalra, and J. G. Moss, "Revascularization versus Medical Therapy for Renal-Artery Stenosis," *New England Journal of Medicine*, vol. 361, no. 20, pp. 1953–1962, 2009.

[21] P. M. van Brussel, T. P. van de Hoef, R. J. de Winter, L. Vogt, and B. J. van den Born, "Hemodynamic Measurements for the Selection of Patients With Renal Artery Stenosis: A Systematic Review," *JACC: Cardiovascular Interventions*, vol. 10, no. 10, pp. 973–985, 2017.

[22] M. W. Burket, C. J. Cooper, D. J. Kennedy, P. S. Brewster, G. M. Ansel, J. A. Moore, J. Venkatesan, and W. L. Henrich, "Renal artery angioplasty and stent placement: Predictors of a favorable outcome," *American Heart Journal*, vol. 139, no. 1 I, pp. 64–71, 2000.

[23] Nefrovisie, "RENINE annual report 2019," tech. rep., 2019.

[24] U. Blum, B. Krumme, P. Flügel, A. Gabelmann, T. Lehnert, C. Buitrago-Tellez, P. Schollmeyer, and M. Langer, "Treatment of Ostial Renal-Artery Stenosis with Vascular Endoprotheses After Unsuccessful Balloon Angioplasty," *New England Journal of Medicine*, vol. 336, no. 7, pp. 459–465, 1997.

[25] P. Harden, M. MacLeod, R. Rodger, G. Baxter, J. Connell, A. Dominiczak, B. Junor, J. Briggs, and J. Moss, "Effect of renal-artery stenting on progression of renovascular renal failure.," *Lancet*, vol. 349, pp. 11333–1136, 1997.

[26] P. S. Watson, P. Hadjipetrou, S. V. Cox, T. C. Piemonte, and A. C. Eisenhauer, "Effect of renal artery stenting on renal function and size in patients with atherosclerotic renovascular disease," *Circulation*, vol. 102, no. 14, pp. 1671–1677, 2000.

[27] C. J. Cooper, T. P. Murphy, D. E. Cutlip, K. Jamerson, W. Henrich, D. M. Reid, D. J. Cohen, A. H. Matsumoto, M. Steffes, M. R. Jaff, M. R. Prince, E. F. Lewis, K. R. Tuttle, J. I. Shapiro, J. H. Rundback, J. M. Massaro, R. B. D'Agostino, and L. D. Dworkin, "Stenting and Medical Therapy for Atherosclerotic Renal-Artery Stenosis," *New England Journal of Medicine*, vol. 370, no. 1, pp. 13–22, 2014.

[28] L. Bax, W. P. Mali, and J. J. Beutler, "Stent placement in patients with atherosclerotic renal artery stenosis and impaired renal function: Response," *Annals of Internal Medicine*, vol. 152, no. 3, p. 198, 2010.

[29] P. M. Van Brussel, M. A. van Lavieren, G. W. Wijntjens, D. Collard, K. P. van Lienden, J. A. Reekers, L. Vogt, J. J. Piek, R. J. de Winter, and B. J. H. van den Born, "Feasibility and reproducibility of renal flow reserve with combined pressure and flow velocity measurements," *EuroIntervention*, vol. 16, no. 12, pp. E1036–E1038, 2020.

[30] S. M. Herrmann and S. C. Textor, "Current Concepts in the Treatment of Renovascular Hypertension," *American Journal of Hypertension*, vol. 31, pp. 139–149, 2 2018.

[31] T. M. Carr, S. S. Sabri, U. C. Turba, A. W. Park, W. E. Saad, J. F. Angle, and A. H. Matsumoto, "Stenting for Atherosclerotic Renal Artery Stenosis," *Techniques in Vascular and Interventional Radiology*, vol. 13, no. 2, pp. 134–145, 2010.

[32] F. Mangiacapra, C. Trana, G. Sarno, G. Davidavicius, M. Protasiewicz, O. Muller, A. Ntalianis, N. Misonis, B. Van Vlem, G. R. Heyndrickx, and B. De Bruyne, "Translesional pressure gradients to predict blood pressure response after renal artery stenting in patients with renovascular hypertension," *Circulation: Cardiovascular Interventions*, vol. 3, pp. 537–542, 12 2010.

[33] M. A. Leesar, J. Varma, A. Shapira, I. Fahsah, S. T. Raza, Z. Elghoul, A. C. Leonard, K. Meganathan, and S. Ikram, "Prediction of Hypertension Improvement After Stenting of Renal Artery Stenosis. Comparative Accuracy of Translesional Pressure Gradients, Intravascular Ultrasound, and Angiography," *Journal of the American College of Cardiology*, vol. 53, pp. 2363–2371, 6 2009.

[34] J. A. Mitchell, R. Subramanian, C. J. White, P. A. Soukas, Y. Almagor, R. E. Stewart, and K. Rosenfield, "Predicting blood pressure improvement in hypertensive patients after renal artery stent placement: Renal fractional flow reserve," *Catheterization and Cardiovascular Interventions*, vol. 69, pp. 685–689, 4 2007.

[35] J. Kadziela, A. Januszewicz, A. Prejbisz, I. Michałowska, M. Januszewicz, E. Florczak, Kalińczuk, B. Norwa-Otto, E. Warchoł, and A. Witkowski, "Prognostic value of renal fractional flow reserve in blood pressure response after renal artery stenting (PREFER study)," *Cardiology Journal*, vol. 20, no. 4, pp. 418–422, 2013.

[36] S. Osher and R. Fedkiw, *Level Set Methods and Dynamic Implicit Surfaces*. 2003.

[37] L. Antiga, M. Piccinelli, L. Botti, B. Ene-Iordache, A. Remuzzi, and D. A. Steinman, "An image-based modeling framework for patient-specific computational hemodynamics," *Medical and Biological Engineering and Computing*, vol. 46, no. 11, pp. 1097–1112, 2008.

[38] M. A. Day, "The No-Slip Condition of Fluid Dynamics," *Erkenntnis (1975-)*, vol. 33, no. 3, pp. 285–296, 1990.

[39] E. Nader, S. Skinner, M. Romana, R. Fort, N. Lemonne, N. Guillot, A. Gauthier, S. Antoine-Jonville, C. Renoux, M. D. Hardy-Dessources, E. Stauffer, P. Joly, Y. Bertrand, and P. Connes, "Blood rheology: Key parameters, impact on blood flow, role in sickle cell disease and effects of exercise," *Frontiers in Physiology*, vol. 10, no. 1329, 2019.

[40] T. Kenner, "The measurement of blood density and its meaning," *Basic research in cardiology*, vol. 84, no. 2, pp. 111–124, 1989.

[41] D. J. Vitello, R. M. Ripper, M. R. Fettiplace, G. L. Weinberg, and J. M. Vitello, "Blood Density Is Nearly Equal to Water Density: A Validation Study of the Gravimetric Method of Measuring Intraoperative Blood Loss," *Journal of Veterinary Medicine*, vol. 2015, pp. 1–4, 1 2015.

[42] A. Updegrove, N. M. Wilson, J. Merkow, H. Lan, A. L. Marsden, and S. C. Shadden, "SimVascular: An Open Source Pipeline for Cardiovascular Simulation," *Annals of biomedical engineering*, vol. 45, no. 3, pp. 525–541, 2017.

[43] N. H. Pijls, J. A. Van Son, R. L. Kirkeeide, B. De Bruyne, and K. L. Gould, "Experimental basis of determining maximum coronary, myocardial, and collateral blood flow by pressure measurements for assessing functional stenosis severity before and after percutaneous transluminal coronary angioplasty," *Circulation*, vol. 87, no. 4, pp. 1354–1367, 1993.

[44] J. Päivärinta, N. Koivuviita, V. Oikonen, H. Iida, K. Liukko, I. Manner, E. Löyttyniemi, P. Nuutila, and K. Metsärinne, "The renal blood flow reserve in healthy humans and patients with atherosclerotic renovascular disease measured by positron emission tomography using [15O]H2O," *EJNMMI Research*, vol. 8, 2018.

[45] S. C. Textor and L. Lerman, "Renovascular hypertension and ischemic nephropathy," *American Journal of Hypertension*, vol. 23, pp. 1159–1169, 11 2010.

[46] A. R. Chade, M. Rodriguez-Porcel, J. P. Grande, X. Zhu, V. Sica, C. Napoli, T. Sawamura, S. C. Textor, A. Lerman, and L. O. Lerman, "Mechanisms of renal structural alterations in combined hypercholesterolemia and renal artery stenosis," *Arteriosclerosis, Thrombosis, and Vascular Biology*, vol. 23, pp. 1295–1301, 7 2003.

[47] D. Sun, A. Eirin, B. Ebrahimi, S. C. Textor, A. Lerman, and L. O. Lerman, "Early atherosclerosis aggravates renal microvascular loss and fibrosis in swine renal artery stenosis," *Journal of the American Society of Hypertension*, vol. 10, pp. 325–335, 4 2016.

[48] Radermacher J, Chavan A, Bleck J, Vitzthum A, Stoess B, Gebel M. J., Galanski M, Kock K. M., and Haller H, "Use of Doppler ultrasonography to predict the outcome of therapy for renal-artery stenosis," *The New England journal of medicine*, vol. 344, no. 6, pp. 410–417, 2001.

[49] I. H. Gong, J. Hwang, D. K. Choi, S. R. Lee, Y. K. Hong, J. Y. Hong, D. S. Park, and H. G. Jeon, "Relationship among total kidney volume, renal function and age," *Journal of Urology*, vol. 187, pp. 344–349, 1 2012.

[50] A. Fedorov, R. Beichel, J. Kalpathy-Cramer, J. Finet, J. C. Fillion-Robin, S. Pujol, C. Bauer, D. Jennings, F. Fennessy, M. Sonka, J. Buatti, S. Aylward, J. V. Miller, S. Pieper, and R. Kikinis, "3D Slicer as an image computing platform for the Quantitative Imaging Network," *Magnetic Resonance Imaging*, vol. 30, pp. 1323–1341, 11 2012.

[51] H.-J. Chang, "Determination of sample size in using central limit theorem for Weibull distribution On sample size for using Central limit theory in various distributions View project," *Information and Management Sciences*, vol. 17, no. 3, pp. 31–46, 2006.

[52] G. Manoharan, N. H. Pijls, N. Lameire, K. Verhamme, G. R. Heyndrickx, E. Barbato, W. Wijns, J. Madaric, X. Tielbeele, J. Bartunek, and B. De Bruyne, "Assessment of renal flow and flow reserve in humans," *Journal of the American College of Cardiology*, vol. 47, pp. 620–625, 2 2006.

[53] C. Ronco, R. Bellomo, and J. Kellum, "Understanding renal functional reserve," *Intensive Care Medicine*, vol. 43, pp. 917–920, 6 2017.

[54] A. Gaipov, Y. Solak, N. Zhampeissov, A. Dzholdasbekova, N. Popova, M. Z. Molnar, S. Tuganbekova, and E. Iskandirova, "Renal functional reserve and renal hemodynamics in hypertensive patients," *Renal Failure*, vol. 38, pp. 1391–1397, 10 2016.

[55] P. Meimoun and C. Tribouilloy, "Non-invasive assessment of coronary flow and coronary flow reserve by transthoracic Doppler echocardiography: A magic tool for the real world," 7 2008.

[56] R. B. Stephenson, "Overview of Cardiovascular Function," in *Cunningham's Textbook of Veterinary Physiology* (B. G. Klein, ed.), pp. 173–185, 2020.

[57] C. A. Taylor, T. J. R. Hughes, and C. K. Zarins, "Effect of exercise on hemodynamic conditions in the abdominal aorta," *Journal of Vascular Surgery*, vol. 29, no. 6, pp. 1077–1089, 1999.

[58] V. Aboyans, J. B. Ricco, M. L. E. Bartelink, and et al., "2017 ESC Guidelines on the Diagnosis and Treatment of Peripheral Arterial Diseases, in collaboration with the European Society for Vascular Surgery (ESVS)," *European Heart Journal*, vol. 39, pp. 763–816, 3 2018.

[59] D. F. Young, "Fluid Mechanics of Arterial Stenoses," *Journal of Biomechanical Engineering*, vol. 101, no. 3, pp. 157–175, 1979.

[60] U. Hoffmann, M. Ferencik, R. C. Cury, and A. J. Pena, "Coronary CT Angiography," *Journal of nuclear medicine*, vol. 47, no. 5, pp. 797–806, 2006.

[61] A. Mandaltsi, A. Grytsan, A. Odudu, J. Kadziela, P. D. Morris, A. Witkowski, T. Ellam, P. Kalra, and A. Marzo, "Non-invasive stenotic renal artery haemodynamics by in silico Medicine," *Frontiers in Physiology*, vol. 9, 8 2018.

[62] D. Chemla, J.-L. He, . Bert, E. Aptecar, J.-X. Mazoit, K. Zamani, R. Frank, G. Fontaine, A. Nitenberg, and Y. Lecarpentier, "Empirical estimates of mean aortic pressure: advantages, drawbacks and implications for pressure redundancy," *Clinical Science*, vol. 103, no. 1, pp. 7–13, 2002.

[63] A. C. Benim, A. Nahavandi, A. Assmann, D. Schubert, P. Feindt, and S. H. Suh, "Simulation of blood flow in human aorta with emphasis on outlet boundary conditions," *Applied Mathematical Modelling*, vol. 35, pp. 3175–3188, 7 2011.

[64] Dalal R, Bruss ZS, and Sehdev JS, "Physiology, Renal Blood Flow and Filtration.," 1 2022.

[65] R. Tricarico, L. Laquian, M. B. Allen, R. Tran-Son-Tay, S. T. Scali, T. C. Lee, A. W. Beck, S. A. Berceli, and Y. He, "Temporal analysis of arch artery diameter and flow rate in patients undergoing aortic arch endograft procedures," *Physiological Measurement*, vol. 41, 3 2020.

[66] R. Revellin, F. Rousset, D. Baud, and J. Bonjour, "Extension of murray's law using a non-newtonian model of blood flow," *Theoretical Biology and Medical Modelling*, vol. 6, no. 1, 2009.

[67] R. S. Reneman and A. P. Hoeks, "Wall shear stress as measured in vivo: Consequences for the design of the arterial system," *Medical and Biological Engineering and Computing*, vol. 46, pp. 499–507, 5 2008.

[68] R. S. Seymour, Q. Hu, and E. P. Snelling, "Blood flow rate and wall shear stress in seven major cephalic arteries of humans," *Journal of Anatomy*, vol. 236, pp. 522–530, 3 2020.

[69] C. Hacking and O. Bashir, "Renal artery," 2 2012.

[70] Leslie SW and Sajjad H, "Anatomy, Abdomen and Pelvis, Renal Artery - PubMed," 2022.

[71] P. M. McGah, J. D. Nerva, R. P. Morton, M. C. Barbour, M. R. Levitt, P. D. Mourad, L. J. Kim, and A. Aliseda, "In vitro validation of endovascular Doppler-derived flow rates in models of the cerebral circulation," *Physiological Measurement*, vol. 36, 10 2015.

[72] J. R. Womersley, "Method for the calculation of velocity, rate of flow and viscous drag in arteries when the pressure gradient is known," *The Journal of Physiology*, vol. 127, pp. 553–563, 3 1955.

[73] T. F. Sherman, "On connecting large vessels to small," *Journal of General Physiology*, vol. 78, no. 4, pp. 431–453, 1981.

[74] G. S. Kassab, "Scaling laws of vascular trees: Of form and function," *American Journal of Physiology - Heart and Circulatory Physiology*, vol. 290, no. 2, pp. 894–903, 2006.

[75] M. Zamir, P. Sinclair, and T. Wonnacott, "Relation between diameter and flow in major branches of the arch of the aorta," *Journal of biomechanics*, vol. 25, no. 11, pp. 1303–1310, 1992.

[76] A. Kamiya and T. Togawa, "Adaptive regulation of wall shear stress to flow change in the canine carotid artery," *The American journal of physiology*, vol. 239, no. 1, 1980.

[77] C. K. Zarins, M. A. Zatina, D. P. Giddens, D. N. Ku, and S. Glagov, "Shear stress regulation of artery lumen diameter in experimental atherogenesis," *Journal of Vascular Surgery*, vol. 5, pp. 413–420, 3 1987.

[78] D. F. Young and F. Y. Tsai, "Flow characteristics in models of arterial stenoses — I. Steady flow," *Journal of Biomechanics*, vol. 6, no. 4, pp. 395–410, 1973.

[79] P. A. Tonino, B. De Bruyne, N. H. Pijls, U. Siebert, F. Ikeno, M. van, V. Klauss, G. Manoharan, T. Engstrøm, K. G. Oldroyd, P. N. Ver Lee, P. A. MacCarthy, and W. F. Fearon, "Fractional Flow Reserve versus Angiography for Guiding Percutaneous Coronary Intervention," tech. rep., 2009.

[80] J. J. Piek, E. Boersma, C. Di Mario, E. Schroeder, C. Vrints, P. Probst, B. De Bruyne, C. Hanet, E. Fleck, M. Haude, E. Verna, V. Voudris, H. Geschwind, H. Emanuelsson, V. Mühlberger, H. O. Peels, and P. W. Serruys, "Angiographical and Doppler flow-derived parameters for assessment of coronary lesion severity and its relation to the result of exercise electrocardiography," *European Heart Journal*, vol. 21, pp. 466–474, 3 2000.

[81] M. Reinhard, K. Schousboe, U. B. Andersen, N. H. Buus, J. M. Rantanen, J. N. Bech, H. M. Mafi, S. Langfeldt, A. Bharadwaz, A. Hørlyck, M. K. Jensen, J. Jeppesen, M. H.

Olsen, I. A. Jacobsen, B. M. Bibby, and K. L. Christensen, "Renal Artery Stenting in Consecutive High-Risk Patients With Atherosclerotic Renovascular Disease: A Prospective 2-Center Cohort Study," *Journal of the American Heart Association*, vol. 11, 4 2022.

[82] M. Law, N. Wald, and J. Morris, "Lowering blood pressure to prevent myocardial infarction and stroke: a new preventive strategy," *Health Technology Assessment*, vol. 7, no. 31, 2003.

[83] P. Y. Courand, M. Dinic, A. Lorthioir, G. Bobrie, C. Grataloup, N. Denarié, G. Soulat, E. Mousseaux, M. Sapoval, M. Azizi, and L. Amar, "Resistant hypertension and atherosclerotic renal artery stenosis effects of angioplasty on ambulatory blood pressure. A retrospective uncontrolled single-center study," *Hypertension*, vol. 74, pp. 1516–1523, 12 2019.

[84] E. Mishima, T. Suzuki, and S. Ito, "Selection of Patients for Angioplasty for Treatment of Atherosclerotic Renovascular Disease: Predicting Responsive Patients," *American Journal of Hypertension*, vol. 33, pp. 391–401, 4 2020.

[85] S. Moccia, E. De Momi, S. El Hadji, and L. S. Mattos, "Blood vessel segmentation algorithms — Review of methods, datasets and evaluation metrics," *Computer Methods and Programs in Biomedicine*, vol. 158, pp. 71–91, 5 2018.

[86] Y. Li, Y. Wu, J. He, W. Jiang, J. Wang, Y. Peng, Y. Jia, T. Xiong, K. Jia, Z. Yi, and M. Chen, "Automatic coronary artery segmentation and diagnosis of stenosis by deep learning based on computed tomographic coronary angiography," *European Radiology*, vol. 32, pp. 6037–6045, 9 2022.

[87] J. Latina, M. Shabani, K. Kapoor, S. P. Whelton, J. C. Trost, J. Sesso, S. Demehri, M. Mahesh, J. A. Lima, and A. Arbab-Zadeh, "Ultra-high-resolution coronary ct angiography for assessment of patients with severe coronary artery calcification: Initial experience," *Radiology: Cardiothoracic Imaging*, vol. 3, no. 4, 2021.

[88] L. M. Trunz and R. Balasubramanya, "Doppler Renal Assessment, Protocols, And Interpretation," *StatPearls*, 6 2022.

[89] C. McArthur and G. M. Baxter, "Current and potential renal applications of contrast-enhanced ultrasound," *Clinical Radiology*, vol. 67, pp. 909–922, 9 2012.

[90] K. Kalantarinia, J. T. Belcik, J. T. Patrie, and K. Wei, "Innovative Methodology Real-time measurement of renal blood flow in healthy subjects using contrast-enhanced ultrasound," *American journal of physiology. Renal physiology*, vol. 297, no. 4, pp. 1129–1134, 2009.

[91] M. W. de Haan, M. Kouwenhoven, A. Kessels, and J. M. van Engelshoven, "Renal artery blood flow: quantification with breath-hold or respiratory triggered phase-contrast MR imaging," *European radiology*, vol. 10, no. 7, pp. 1133–1137, 2000.

[92] A. L. Wentland, T. M. Grist, and O. Wieben, "Repeatability and Internal Consistency of Abdominal 2D and 4D Phase Contrast MR Flow Measurements," *Academic Radiology*, vol. 20, pp. 699–704, 6 2013.

[93] D. Motoyama, Y. Ishii, Y. Takehara, M. Sugiyama, W. Yang, H. Nasu, T. Ushio, Y. Hirose, N. Ohishi, T. Wakayama, H. Kabasawa, K. Johnson, O. Wieben, H. Sakahara, and S. Ozono, "Four-dimensional phase-contrast vastly undersampled isotropic projection reconstruction (4D PC-VIPR) MR evaluation of the renal arteries in transplant recipients: Preliminary results," *Journal of Magnetic Resonance Imaging*, vol. 46, pp. 595–603, 8 2017.

[94] M. Korkmaz, B. Aras, S. Güneyli, and M. Yılmaz, "Clinical significance of renal cortical thickness in patients with chronic kidney disease," *Ultrasonography*, vol. 37, pp. 50–54, 1 2018.